iScience

CellPress
OPEN ACCESS

Article

Distinct niche structures and intrinsic programs of fallopian tube and ovarian surface epithelial cells

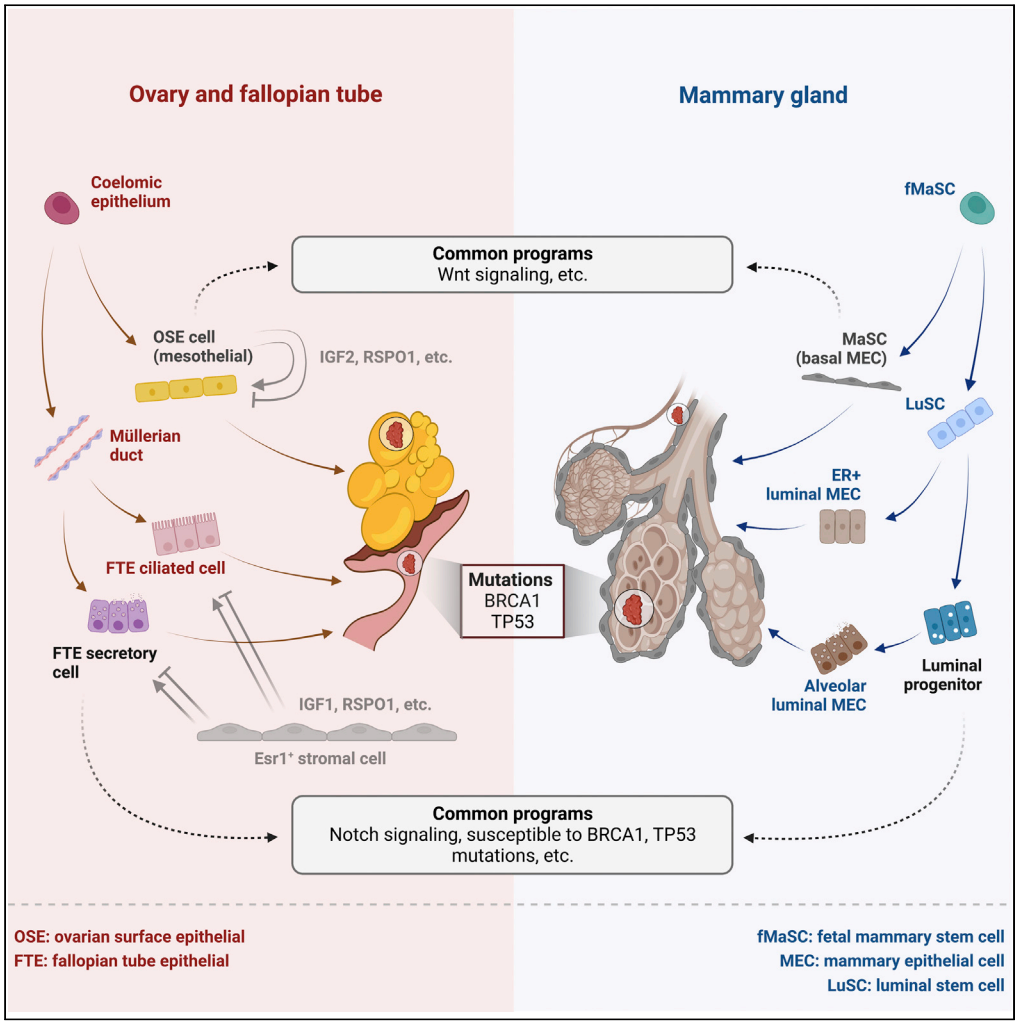

Guyu Qin, Eun-Sil Park, Xueqing Chen, ..., Huidong Chen, Guo-Cheng Yuan, Zhe Li

zli4@rics.bwh.harvard.edu

Highlights

Fallopian tube secretory stem/progenitor cells resemble mammary luminal progenitors

Esr1^{+} stromal cells serve as a potential niche for fallopian tube epithelial cells

IGF1 is a niche factor supporting fallopian tube epithelial growth/differentiation

Ovarian surface epithelial cells resemble basal cells and may serve as own niche

Qin et al., iScience *26*, 105861
January 20, 2023
https://doi.org/10.1016/j.isci.2022.105861

iScience

CellPress
OPEN ACCESS

Article

Distinct niche structures and intrinsic programs of fallopian tube and ovarian surface epithelial cells

Guyu Qin,[1,2,4] Eun-Sil Park,[1,2,4] Xueqing Chen,[1,2,4] Sen Han,[1,2] Dongxi Xiang,[1,2] Fang Ren,[1] Gang Liu,[1] Huidong Chen,[3] Guo-Cheng Yuan,[3] and Zhe Li[1,2,*]

SUMMARY

Epithelial ovarian cancer (EOC) can originate from either fallopian tube epithelial (FTE) or ovarian surface epithelial (OSE) cells, but with different latencies and disease outcomes. To address the basis of these differences, we performed single cell RNA-sequencing of mouse cells isolated from the distal half of fallopian tube (FT) and surface layer of ovary. We find at the molecular level, FTE secretory stem/progenitor cells and OSE cells resemble mammary luminal progenitors and basal cells, respectively. An FT stromal subpopulation, enriched with *Pdgfra*$^+$ and *Esr1*$^+$ cells, expresses multiple secreted factor (e.g., IGF1) and Hedgehog pathway genes and may serve as a niche for FTE cells. In contrast, *Lgr5*$^+$ OSE cells express similar genes largely by themselves, raising a possibility that they serve as their own niche. The differences in intrinsic expression programs and niche organizations of FTE and OSE cells may contribute to their different courses toward the development of EOCs.

INTRODUCTION

Epithelial ovarian cancer (EOC) is the most lethal malignancy of the female reproductive system, largely because of the fact that most EOCs are diagnosed only after the cancer has metastasized into the peritoneal space of patient.[1,2] Although the overall survival rate 5 years after the diagnosis throughout the world is around 46%, it is reduced to only ~29% when the cancer is detected at the late stage.[2] Thus, to improve EOC patient outcome, a major challenge is to understand the early stage of the disease. EOCs are classified as several histologic subtypes,[3,4] which resemble the Müllerian duct-derived fallopian tube (FT) (serous EOC), endometrium (endometrioid EOC), endocervix (mucinous EOC), or vagina (clear cell EOC). The most common subtype is serous EOC, which is an aggressive type of EOC with high fatality, and typically carries *TP53* mutations[4,5]; this is also the EOC subtype often developed in *BRCA1* and *BRCA2* mutation carriers.

The cellular origin of EOCs has been a topic of long-standing debate.[6] In one view, it is proposed that EOCs are derived from transformation of ovarian surface epithelium, a layer of less differentiated epithelial cells lining the ovarian surface (OS) and inclusion cysts within ovaries. The incompletely committed and multipotential nature of ovarian surface epithelial (OSE) cells potentially provides a cellular basis for the phenotypic diversity observed in EOCs. In a second view, it is proposed that EOCs may originate from the fimbrial epithelial cells of the FT that later metastasize to the OS. This view is mainly supported by the precursor lesions [e.g., serous tubal intraepithelial carcinoma (STIC)[7,8]] detected in the fimbrial portion of the FT observed in ovarian cancer patients, in particular in those with germline *BRCA1* mutations. It is also supported by several genetically engineered mouse models in which transformation of fallopian tube epithelial (FTE) cells led to development of EOCs.[9–11] More recently, evidence from mouse models, largely based on organoids derived from FTE and OSE cells, respectively, further supported the dual origins of EOCs; specifically, it was shown that both FTE and OSE cells could serve as cells-of-origin of high-grade serous ovarian cancers (HGSOCs).[12,13]

Of note, when the same genetic lesions commonly found in human HGSOCs were engineered into murine FTE and OSE cells *in vivo* or *in vitro* (into their corresponding organoid cells), both types of mutated cells could form HGSOCs *in situ* or on transplantation.[12,13] However, the mutated FTE cells formed malignant tumors with a shorter latency and higher penetrance than OSE cells; in addition, the mutated cells also

[1]Division of Genetics, Brigham and Women's Hospital, Boston, MA 02115, USA

[2]Department of Medicine, Harvard Medical School, Boston, MA 02115, USA

[3]Department of Biostatistics and Computational Biology, Dana-Farber Cancer Institute, Harvard School of Public Health, Boston, MA 02215, USA

[4]These authors contributed equally

*Correspondence: zli4@rics.bwh.harvard.edu

https://doi.org/10.1016/j.isci.2022.105861

exhibited distinct cellular origin-dependent chemosensitivities.[12,13] These differences could be because of intrinsic lineage-specific differences in FTE and OSE cells, particularly their corresponding stem/progenitor cells, which often serve as cell-of-origin of cancer.[14] OSE homeostasis and ovulatory regenerative repair are maintained by LGR5$^+$ OSE cells.[15,16] FT epithelium is sustained by FTE stem/progenitor cells in the secretory cell lineage.[17] The difference could also be attributed to distinct regulations of OSE and FTE stem/progenitor cells by their corresponding niches. The fate and homeostasis of epithelial cells are dominantly controlled by their supporting cells, or niche, which produces secreted factors to regulate both stem cell self-renewal and differentiation via signaling pathways.[18–20] Loss of proper control of epithelial stem/progenitor cell behaviors by their niche can facilitate malignant growth of epithelial cells.[20]

Currently, very little is known about any difference in the intrinsic programs and niches that regulate OSE and FTE stem/progenitor cells. A better understanding of this is crucial for gaining insights into how distinct cells-of-origin of EOCs contribute to different disease latencies and outcomes. To address this, we performed single cell RNA-sequencing (scRNA-seq) of cells isolated from mouse FTs (i.e., oviducts) and ovaries. Analyses and comparison of these data revealed that at the molecular level, FTE secretory stem/progenitor cells and OSE cells resemble luminal progenitors (LPs) and basal cells in the mammary gland, respectively. Furthermore, we identified a subset of FT stromal cells expressing *Pdgfra* and *Esr1*, as well as multiple secreted factor (e.g., *Igf1*, *Rspo1*) and Hedgehog pathway (e.g., *Smo*) genes. We provided experimental evidence to support that FT stromal cells may serve as a niche for FTE cells. In contrast, we found that *Lgr5*$^+$ OSE cells express similar genes largely by themselves, thus raising a possibility that they serve as their own niche. We conclude that the differences in intrinsic expression programs and niche organizations of FTE and OSE cells may contribute to their different courses toward the development of EOCs.

RESULTS

Summary of scRNA-seq data

Mouse and laying hen are commonly used animal models for studying human ovarian cancer.[21,22] As both FTE and OSE cells in mice have clearly been shown to serve as cells-of-origin of EOCs, we focused on mouse as the model system here. To perform single cell expression analysis of FT and ovary and to compare their transcriptomes, we isolated FT and ovarian tissues from two wild-type (WT) adult FVB female mice. For FT, we cut each FT into two-halves and only subjected the distal half (i.e., the portion close to ovary, thus including the fimbrial region, Figure 1A) to single cell preparation. For ovary, we stripped the surface layer of each ovary (i.e., OS) via enzymatic digestion and prepared single cell suspension, which is enriched with OSE cells (Figure 1A). We used the inDrop platform[23] to barcode single cells from FT and OS samples; the resulting expression libraries were then subjected to high throughput sequencing. On resolution of various barcodes and generation of expression matrix for individual cells, we utilized the Seurat single cell data analysis tool[24] to integrate and analyze the expression dataset. The estimated number of cells, total number of genes, median number of genes per cell, and median UMI counts per cell for each sample are summarized in Figure S1A. We performed additional quality control (QC) to filter out doublets or multiplets, as well as damaged or dead cells (Figure S1B). From the remaining FT and OS single cells, we generated cell clusters by using the non-linear dimensional reduction approach Uniform Manifold Approximation and Projection (UMAP). Because single cells from the two biological replicates of each organ clustered together tightly (Figure S1C), we pooled single cells from both FT (i.e., FT#1 and FT#2 as FT) or OS (i.e., OS#1 and OS#2 as OS) samples in all subsequence analyses.

UMAP analysis of the all-in-one dataset revealed eight cell clusters (Figure 1B, marker genes enriched in each cluster are shown in Table S1). Single cells from FT and OS samples only exhibited minimal overlapping in the UMAP 2-Dimensional space (Figure 1C), suggesting distinct transcriptomes of cells from these two organs. Among cell clusters, clusters #0, 3, 4, 6 and 7 mainly included cells from the FT samples, with clusters #6 and 7 composed of only FT cells; clusters #1 and 5 mainly included cells from the OS samples, with cluster #5 composed of only OS cells (Figures 1D and S1D). A quick examination of these cell clusters based on well-known marker genes (e.g., based on The Human Protein Atlas[25]) revealed that clusters #0, 4 and 6 contained FTE secretory cells (based on *Ovgp1*, *Pax8*), cluster #7 contained FTE ciliated cells (*Foxj1*), cluster #5 contained OSE cells (*Lgr5*, *Aldh1a2*), and clusters #1 and 3 were probably enriched with various stromal cells in the FT tissue (*Col1a2*, *Spp1*); of note, cluster #1 may also contain granulosa (*Hsd17b1*) and stromal/theca (*Cyp11a1*) cells in the ovary (Figure 1E). Lastly, cluster #2 contained relatively equal number

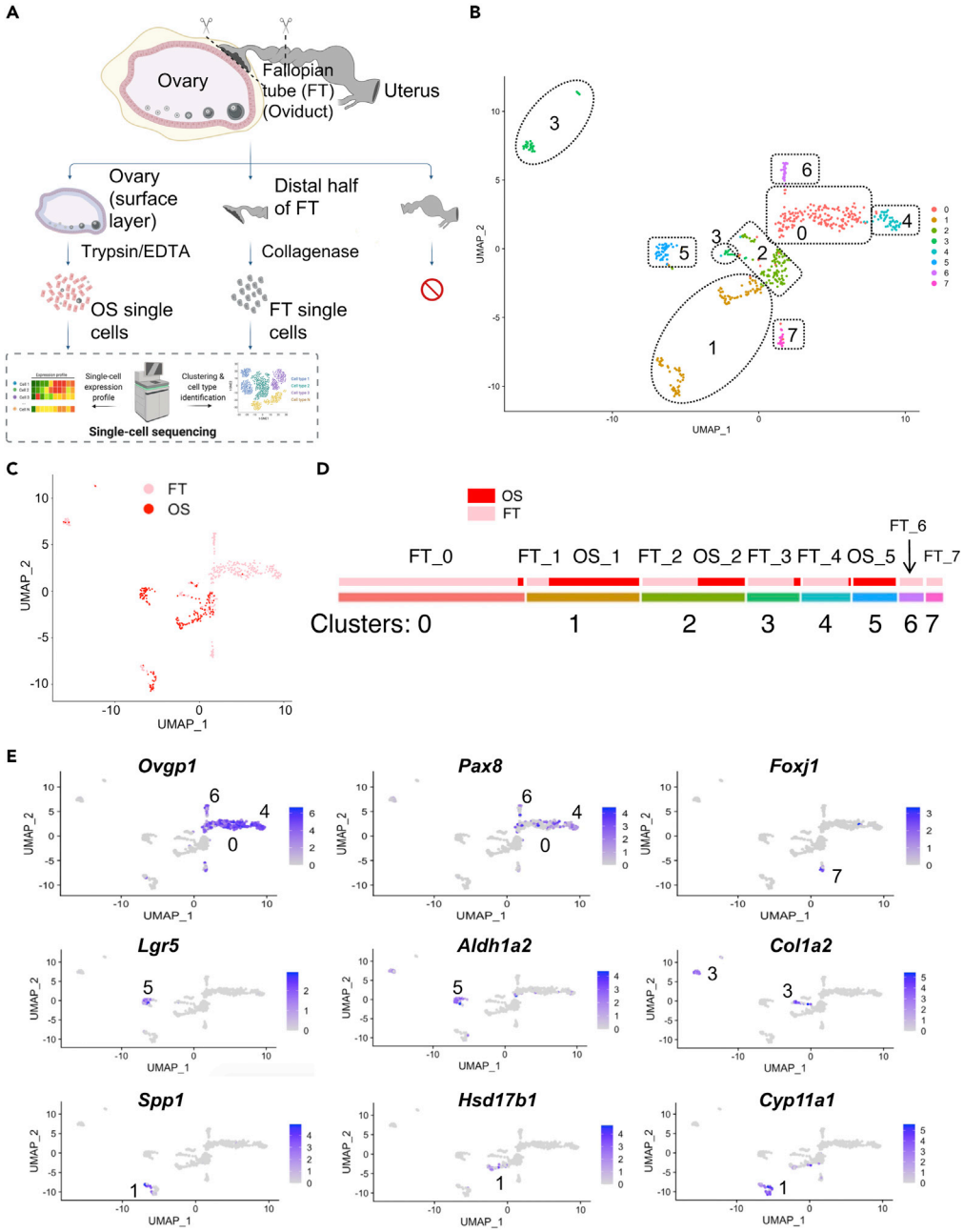

Figure 1. scRNA-seq identified distinct cell populations in FT and OS tissues

(A) Schematic diagram showing the types of FT and OS tissues used for making single cell suspensions and subsequent scRNA-seq.

(B) Eight distinct clusters were identified from FT and OS single cells by using UMAP clustering.

(C) UMAP clusters in (B) were labeled to show their FT or OS sample identity.

(D) Summary of eight cell clusters (0–7) and composition of FT and/or OS cells in each cluster; labels for FT or OS subsets within each cluster (if any) are also shown.

(E) Heatmaps showing expression of representative marker genes in various cell clusters in the UMAP plot as in (B).

See also Figure S1 and Table S1.

of cells from both FT and OS samples. Of note, we noticed top enriched genes of this cluster were mainly hemoglobin (Hbb)-related genes (Figure S1E); violin plot further confirmed that many cells within this cluster expressed high levels of Hbb genes (Figure S1F), suggesting cluster #2 was largely composed of hematopoietic cells, particularly erythrocytes. We thus excluded this cluster in subsequent analyses.

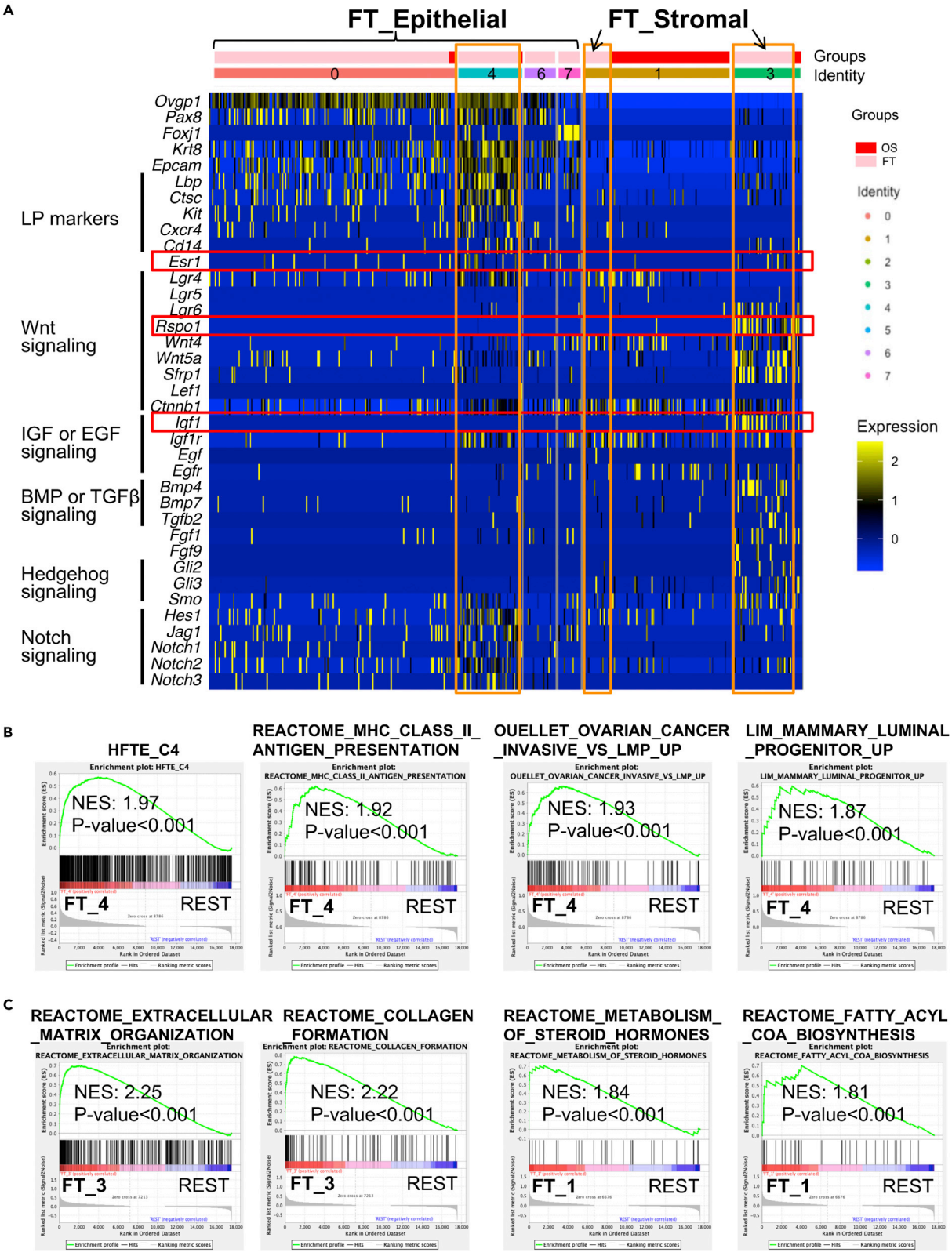
A
FT_Epithelial
FT_Stromal
Groups
Identity
0
4
6
7
1
3
Ovgp1
Pax8
Foxj1
Krt8
Epcam
Lbp
Ctsc
Kit
Cxcr4
Cd14
Esr1
Lgr4
Lgr5
Lgr6
Rspo1
Wnt4
Wnt5a
Sfrp1
Lef1
Ctnnb1
Igf1
Igf1r
Egf
Egfr
Bmp4
Bmp7
Tgfb2
Fgf1
Fgf9
Gli2
Gli3
Smo
Hes1
Jag1
Notch1
Notch2
Notch3
LP markers
Wnt signaling
IGF or EGF signaling
BMP or TGFβ signaling
Hedgehog signaling
Notch signaling
Groups
OS
FT
Identity
0
1
2
3
4
5
6
7
Expression
2
1
0
B
HFTE_C4
NES: 1.97
P-value<0.001
FT_4
REST
REACTOME_MHC_CLASS_II_ANTIGEN_PRESENTATION
NES: 1.92
P-value<0.001
FT_4
REST
OUELLET_OVARIAN_CANCER_INVASIVE_VS_LMP_UP
NES: 1.93
P-value<0.001
FT_4
REST
LIM_MAMMARY_LUMINAL_PROGENITOR_UP
NES: 1.87
P-value<0.001
FT_4
REST
C
REACTOME_EXTRACELLULAR_MATRIX_ORGANIZATION
NES: 2.25
P-value<0.001
FT_3
REST
REACTOME_COLLAGEN_FORMATION
NES: 2.22
P-value<0.001
FT_3
REST
REACTOME_METABOLISM_OF_STEROID_HORMONES
NES: 1.84
P-value<0.001
FT_1
REST
REACTOME_FATTY_ACYL_COA_BIOSYNTHESIS
NES: 1.81
P-value<0.001
FT_1
REST

Figure 2. Summary of FT epithelial and stromal cell clusters

(A) A heatmap showing expression of representative genes in clusters enriched with FTE cells (0, 4, 6, 7) and those enriched with FT stromal cells (1, 3).

(B) GSEA showing enrichment of representative gene sets in FTE secretory cells in the FT_4 sub-cluster. NES: normalized enrichment score.

(C) GSEA showing representative gene sets enriched in two FT stromal cell subsets (FT_3, FT_1).

See also Figures S2 and S3.

FTE cell clusters

Next, we further analyzed cell types in the distal half of the FT. Expression of epithelial cell marker *Krt8* and *Epcam* revealed that FTE cells were distributed among clusters #0, 4, 6 and 7 (Figure 2A). By using the well-established markers for FTE secretory (e.g., *Ovgp1*, *Pax8*) and ciliated (e.g., *Foxj1*) cells, we found that clusters #0, 4, and 6 were mainly composed of *Ovgp1*$^{+}$*Pax8*$^{+}$ secretory cells, whereas cluster #7 was composed of *Foxj1*$^{+}$ ciliated cells (Figure 2A). To more systematically define the cell identities in each cluster, we generated expression data for different subsets of cells in each cluster (if any) based on their tissue of origin (Figure 1D; e.g., FT_1 or OS_1 represent cells in cluster #1 from FT or OS tissues, respectively). By gene set enrichment analysis (GSEA),[26] we confirmed significant enrichment of various cilia-related gene sets in FT_7 cells (Figure S2A). By comparing to gene expression signatures of various human FTE subpopulations from a recent single cell study,[27] we observed profound enrichment of gene sets for human ciliated cell subpopulations 3, 4, 1, and to a lesser degree, subpopulation 2, in FT_7 cells (Figure S2B). This comparison suggests that murine FT_7 ciliated cells from our study closely resemble human partially (ciliated_3) and fully (ciliated_4) differentiated FTE ciliated cells.[27]

To determine the identities of various secretory cell subsets in clusters #0, 4, and 6, we performed cross-species comparisons with FTE cell subsets in normal human FT tissues defined by scRNA-seq from two recent studies.[27,28] By GSEA, we found that FT_4 cells most closely resembled the human FTE C4 subtype from the Hu et al. 2020 study (i.e., KRT17 cluster) (Figures 2B and S2C), which is a cluster highly expressing MHC-II genes, KRT17/23, and ALDH genes, and may represent an FTE progenitor population.[28] Consistently, we found multiple stem/progenitor cell genes [e.g., similar to those expressed in mammary epithelial LPs,[29] such as *Lbp*, *Ctsc*, *Kit*, *Cxcr4*, *Cd14*] were highly expressed in murine FTE cells in cluster #4 (Figure 2A). Furthermore, by GSEA, we found gene sets related to MHC-II/antigen presentation, mammary LPs, and invasive EOCs were also significantly enriched in this cluster (FT_4, Figure 2B). At the pathway level, we found that gene sets related to metabolism, transport, and infection were among top-enriched gene sets (Figure S2D). The enrichment of infection-related gene sets may be because of higher expression levels of immune-related genes (e.g., in sensing bacterial infection) in FTE cells in cluster #4. Lastly, GSEA also revealed that FT_4 cells most closely resembled human FTE secretory clusters 2 and 3 from the Dinh et al. 2021 study (Figure S2E), which may represent committed and early progenitor cells in the secretory lineage, respectively.[27] Lastly, FT_0 and FT_6 cells had low library complexity and exhibited positive enrichment of human FTE C1 (Figure S2C), which together with human FTE C2 (both also exhibited low library complexity), may represent quiescent populations because of cell senescence or loss of hormonal influence.[28] A comparison to the Dinh et al. 2021 revealed that both FT_0 and FT_6 cells most closely resembled human secretory cluster 1 (Figure S2E), which may represent the most differentiated secretory cells.[27] Collectively, these expression analysis and cross-species comparisons suggest that: (1) FT_4 cells may represent FTE stem/progenitor cells in the secretory lineage, whereas FT_0 and FT_6 cells, which appear to include more than half of FTE cells, may represent quiescent/differentiated secretory cells; (2) major FTE subpopulations are conserved between human and mouse. Of note, a recent study demonstrated that mouse FTE (oviduct epithelial) cells constitute two developmental distinct lineages spatially separated along the distal and proximal regions.[30] As our scRNA-seq data was collected from the distal half of the FT, FTE cells in our dataset likely reflect the distal FTE lineage, which could be uniquely susceptible to EOC initiation.

FT stromal cell clusters

In the remaining two clusters (#1, #3) containing FT cells, we found FT_1 and FT_3 cells were largely negative for epithelial markers (e.g., *Krt8*, *Epcam*) and FTE markers (e.g., *Ovgp1*, *Pax8*, *Foxj1*) (Figure 2A), suggesting they may represent two FT stromal cell subpopulations. Importantly, we found many genes encoding secreted growth factors and signaling molecules were expressed in FT stromal cells, particularly in those from cluster #3 (Figure 2A). In FT_3 stromal cells, we found that many of them expressed R-spondin1 (encoded by *Rspo1*), a key agonist for Wnt signaling[31]; of note, stromal cells in FT_3 also appeared to be the only cell population in the FT that expressed *Rspo1* and *Rspo1* was also the main *Rspo* gene expressed

in the FT. In addition, FT_3 stromal cells also expressed additional secreted factor genes that may regulate homeostasis of the nearby FTE cells by various pathways (e.g., *Wnt4/5a* for Wnt signaling, *Igf1* for IGF/IGF1R signaling, *Bmp4/7* for BMP signaling, Figure 2A), thus raising an intriguing possibility that they may constitute a niche for maintaining the FT epithelium. Of note, we found that some FT stromal cells in cluster #3 (but not in cluster #1) also express *Esr1* (Figure 2A), suggesting that FT_3 stromal cells may include a subpopulation of hormone receptor-positive (HR^+) stromal cells. We stained FT tissue sections for estrogen receptor alpha (ERα), and found that in addition to $ER\alpha^+$ FTE cells, many stromal cells with flat nuclei were also $ER\alpha^+$, whereas those with round nuclei were typical $ER\alpha^-$ (Figure S3A). Of note, human FT sections (from *BRCA1/2*mutation carriers) also exhibited a similar stromal ERα staining pattern.[32]

At the pathway level, GSEA revealed gene sets related to extracellular matrix (ECM), collagens, and immune response (e.g., complement) were among the top enriched ones in FT_3 cells, whereas gene sets related to metabolism (e.g., PPAR signaling, steroid hormones, fatty acid biosynthesis) were enriched in FT_1 cells (Figures 2C, S3B, and S3C). In addition, a direct comparison of FT_3 to FT_1 stromal cells revealed that FT_3 stromal cells expressed multiple muscle contraction-related genes at higher levels than those in FT_1 (Figure S3D), suggesting that many FT_3 cells may represent myofibroblasts. Of note, myofibroblasts have been shown as niche cells for multiple epithelial stem cell types (e.g., intestinal, lung alveolar type 2, gastric).[33–36] Importantly, in a recent study of scRNA-seq analysis for human FTs, among FT stromal cells, *ESR1* is expressed at the highest level in a cluster of myofibroblasts,[37] suggesting that the $ER\alpha^+$ FT myofibroblasts are conserved between mouse and human.

Cell surface markers for enriching FT cell subpopulations

Next, we wanted to define cell surface markers so that we could further sort and analyze different subpopulations of cells in the FT by flow cytometry (FACS). To achieve this, we examined our scRNA-seq dataset for differential expression of cell surface marker genes in different FT cell subsets. We found *Cd24a* (encoding CD24) was expressed in most FTE cells in clusters #0, 4, 6, and 7, but not expressed in FT stromal cells in clusters #1 and 3 (Figure 3A). Among FTE cells, *Ceacam1* (encoding CD66a) was expressed in most secretory cells in clusters #0, 4 and 6, but not expressed in ciliated cell-enriched cluster #7 (Figure 3A). Among FT stromal cells in clusters #1 and 3, we found *Pdgfra* (encoding CD140a) was only expressed in many FT_3 cells, whereas *Itgb3* (encoding CD61) was mainly expressed in FT_1 cells (Figure 3A). Based on this expression pattern, we developed a FACS analysis scheme (Figure 3B): we first gated for lineage-negative (Lin^-, i.e., negative for leukocyte marker CD45, endothelial cell marker CD31, and erythrocyte marker TER119) cells prepared from the FT tissue; we then separated Lin^- cells as $CD24^+$ and $CD24^-$ subsets, representing FTE cells and FT stromal cells, representatively. Among Lin^-CD24^+ FTE cells, we further separated them as the $CD66a^+$ and $CD66a^-$ subsets, which were enriched with secretory and ciliated cells, respectively. Among Lin^-CD24^- stromal cells, we further separated them as the $CD140a^+CD61^-$ and $CD140a^-CD61^+$ subsets, which represented two distinct stromal cell subpopulations (corresponding to FT_3 and FT_1 cells, respectively). As CD140a and CD61 appeared to mark these two stromal cell subpopulations in a largely mutually exclusive manner and as $CD140a^+$ cells appeared to be the main stromal cell type (in FT_3 sub-cluster) that produces many secreted factors (Figure 2A), we focused on CD140a and reasoned that the use of CD140a alone would be sufficient to separate these two stromal cell subsets. We verified this scheme by FACS analysis of freshly prepared single cell suspension from FT tissues (Figure 3C). We then sorted these distinct FT epithelial and stromal cell subpopulations based on this FACS scheme and by qRT-PCR analysis, we confirmed higher expression of secretory cell markers *Pax8* and *Ovgp1* in the $CD66a^+$ subset and higher expression of ciliated cell marker *Foxj1* in the $CD66a^-$ subset (Figure S4A and Table S2); we also confirmed higher expression levels of *Esr1*, *Rspo1*, *Lgr6*, *Wnt4*, *Wnt5a* in $CD140a^+$ stromal cells (Figure S4B and Table S2). To further validate the FT stromal subpopulations, we took advantage of a Cre-expressing transgenic mouse line under the control of the *Pdgfra* promoter[38] and coupled it with a conditional Cre-reporter *Rosa26-LSL-YFP* (*R26Y*) [39]; in the resulting *Pdgfra-Cre;R26Y* female mice, we performed FACS analysis of their FT tissues and confirmed that YFP^+ cells largely stained positive for CD140a (Figure S4C).

A potential stromal niche for FTE cells

Our expression analysis of FT single cells suggested that FT stromal cells, particularly those from cluster #3, may constitute a niche for maintaining the FT epithelium. To test this, we examined whether FT stromal cells could support growth/survival of FTE cells *ex vivo* in an organoid culture setting. We previously established an organoid culture system for FTE cells and defined the minimal factor requirement for maintaining FTE organoids long-term (i.e., organoid culture minimal medium containing B27, EGF and TGFBR1 kinase

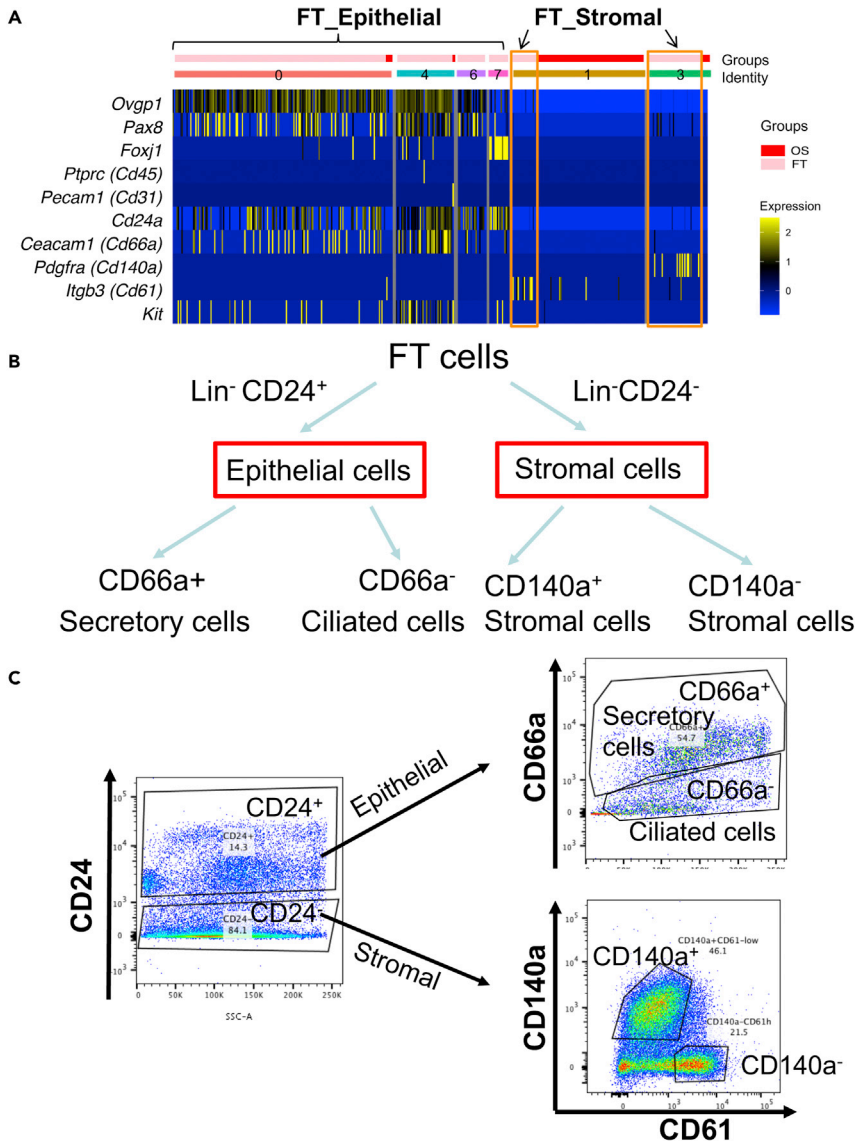

Figure 3. FACS analysis of FT cell populations based on cell surface markers defined by scRNA-seq

(A) A heatmap showing differential expression of several cell surface marker genes in clusters enriched with FTE cells (0, 4, 6, 7) and those enriched with FT stromal cells (1, 3).

(B) Proposed FACS scheme showing analysis of FT epithelial and stromal cell subpopulations based on cell surface markers defined in (A).

(C) FACS analysis of freshly prepared single cell suspension from FT tissues based on the scheme in (B).

See also Figure S4 and Table S2.

inhibitor, referred to as BET medium).[40] Utilizing this platform, we FACS-sorted Lin$^-$CD24$^+$ FTE cells and Lin$^-$CD24$^-$ stromal cells from FTs of WT adult female mice and subjected them to organoid culture (technically, because of the small number of cells we could obtain from each FT, we sorted stromal cells from the Lin$^-$CD24$^-$ gate rather the Lin$^-$CD24$^-$CD140a$^+$ subset). Next, we cultured the freshly sorted Lin$^-$CD24$^+$ FTE cells in the BET medium (initially in the presence of ROCK inhibitor), either alone or together with Lin$^-$CD24$^-$ stromal cells. We found that co-culture with stromal cells led to formation of significantly larger and more organoids from FTE cells than those from FTE cells alone (Figures 4A–4C). Of note, we also confirmed that the sorted Lin$^-$CD24$^-$ cell population (enriched with FT stromal cells) did not form organoid (Figure 4A, right). Together, these data suggest that FT stromal cells support growth/survival of primary FTE cells in the organoid culture setting (i.e., P0 organoids).

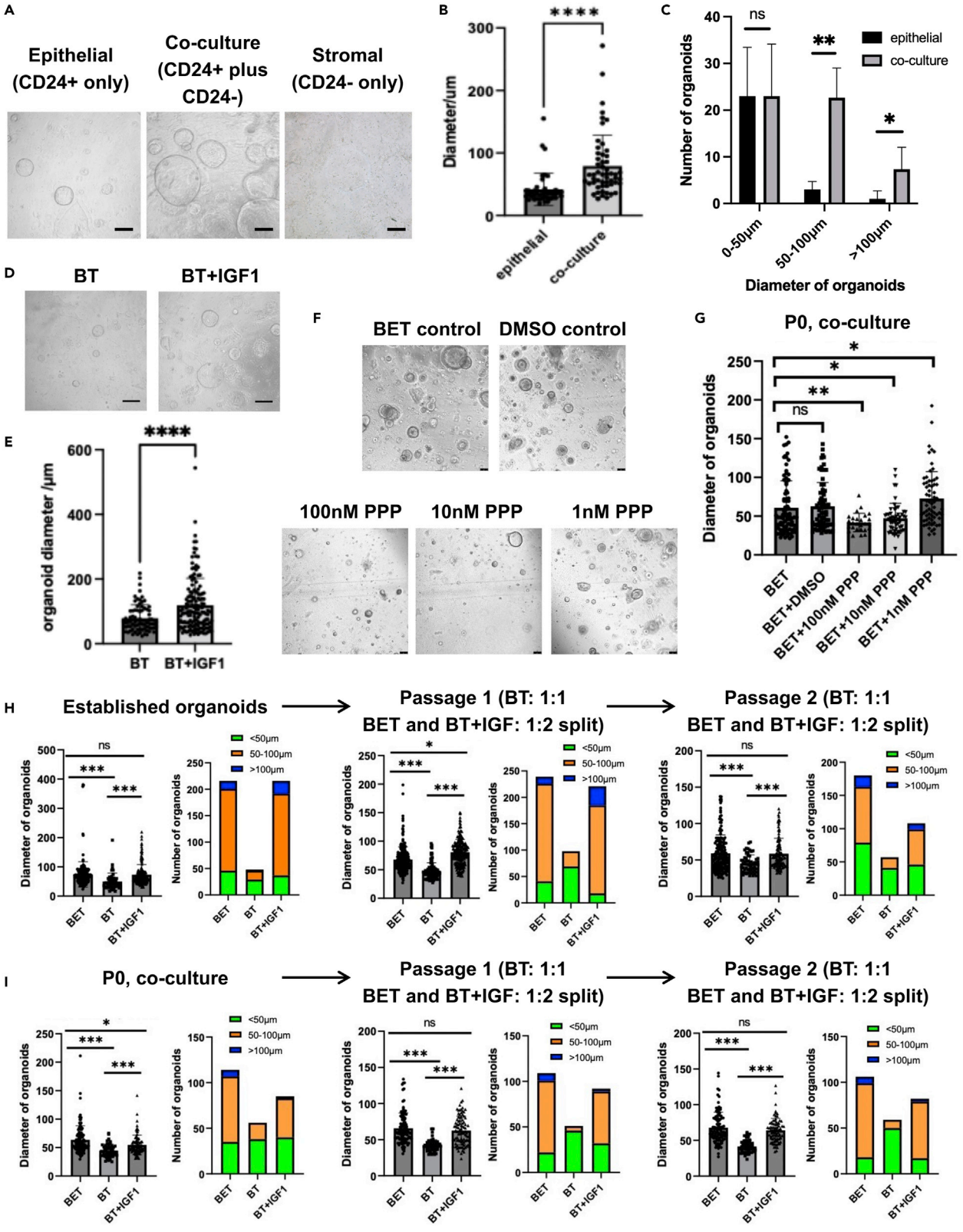
A
Epithelial (CD24+ only)
Co-culture (CD24+ plus CD24-)
Stromal (CD24- only)
B
****
Diameter/um
epithelial
co-culture
C
ns
**
*
epithelial
co-culture
Number of organoids
0-50μm
50-100μm
>100μm
Diameter of organoids
D
BT
BT+IGF1
E
****
organoid diameter /μm
BT
BT+IGF1
F
BET control
DMSO control
100nM PPP
10nM PPP
1nM PPP
G
P0, co-culture
Diameter of organoids
BET
BET+DMSO
BET+100nM PPP
BET+10nM PPP
BET+1nM PPP
H
Established organoids
Passage 1 (BT: 1:1 BET and BT+IGF: 1:2 split)
Passage 2 (BT: 1:1 BET and BT+IGF: 1:2 split)
Diameter of organoids
Number of organoids
<50μm
50-100μm
>100μm
BET
BT
BT+IGF1
I
P0, co-culture
Passage 1 (BT: 1:1 BET and BT+IGF: 1:2 split)
Passage 2 (BT: 1:1 BET and BT+IGF: 1:2 split)

Figure 4. FT stromal cells serve as a niche for FTE cells

(A) Representative pictures from organoid culture of sorted $Lin^{-}CD24^{+}$ cells (4,000, enriched with FTE cells), or $Lin^{-}CD24^{-}$ cells (5,000, enriched with FT stromal cells), or $Lin^{-}CD24^{+}$ cells (4,000) plus $Lin^{-}CD24^{-}$ cells (5,000) (co-culture), scale bar = 100 μm.

(B) Quantification of sizes of organoids for (A); ****: $p \leq 0.0001$.

(C) Quantification of numbers of organoids (at different size ranges) formed from different cultures as in (A). Data are represented as mean ± SEM from three independent experiments; **: $p \leq 0.01$, *: $p \leq 0.05$, ns: not significant.

(D) Representative pictures from organoid culture of sorted $Lin^{-}CD24^{+}$ cells (4,000) in the BT medium in the absence (control) or presence of IGF1, scale bar = 100 μm.

(E) Quantification of sizes of organoids for (D); ****: $p \leq 0.0001$.

(F) Representative pictures from organoid co-culture in the presence (or absence, or DMSO vehicle control) of different concentrations of the IGF1R inhibitor, PPP, scale bar = 100 μm.

(G) Quantification of sizes of organoids for (F); **: $p \leq 0.01$, *: $p \leq 0.05$, ns: not significant.

(H and I) Quantification of sizes and numbers of organoids at different passages of the long-term culture, started from either established organoids (i.e., established via serial passages in the BET medium) (H) or P0 organoid co-culture (i.e., FTE cells + stromal cells from fresh FT tissues) (I), under either the BET, or BT, or BT + IGF1 medium. During each passage, organoids in the BET or BT + IGF1 medium were split at a 1:2 ratio; under the BT medium, because of the small cell number, all recovered single cells were passaged to the next round (1:1). Organoid cells were allowed to grow for 7 days and were then passaged. ***: $p \leq 0.001$, *: $p \leq 0.05$, ns: not significant.

See also Figure S5.

Surprisingly, when we co-cultured established FTE organoid cells (i.e., via >5 serial passages in the BET medium) with freshly sorted $Lin^{-}CD24^{-}$ FT stromal cells, we only observed a slight increase in the organoid size when compared to the FTE-only control, and the size difference did not reach statistical significance (Figure S5A). To determine if this was because of a difference in the cell composition in the established versus P0 organoids, we performed FACS analysis. We found that P0 organoids formed from freshly prepared single cells from FT tissues contained both $Lin^{-}CD24^{+}CD66a^{+}$ and $Lin^{-}CD24^{+}CD66a^{-}$ organoid cells (Figure S5B), which are enriched with secretory and ciliated cells, respectively (Figure 3). However, via serial passage in the BET medium, we found that the established organoids were composed of largely $Lin^{-}CD24^{+}CD66a^{+}$ secretory cells (Figure S5C). These data suggested that: (1) the factors in the minimal BET medium were sufficient to sustain growth/survival of FTE secretory cells *ex vivo* so that factors produced by FT stromal cells had minimal effects on them; (2) in contrast, ciliated cells (which represent more differentiated FTE cells[17]) were not maintained long-term in the BET medium and additional factors from the FT stromal cells may be required to support their growth/survival (or to maintain their differentiation state).

Among secreted factors that can be produced by FT stromal cells (e.g., by FT_3 cells, Figure 2A), BMP4 and BMP7 are known factors required for epithelial stem cell differentiation.[20] We reported previously that addition of the Wnt agonist R-spondin1 to the BET medium led to formation of FTE organoids with more differentiated ciliated cells.[40] Of interest, we observed that addition of the Porcupine inhibitor (e.g., LGK-974, IWP2), which inhibits Wnt signaling (by blocking processing and secretion of the endogenous Wnt proteins),[41] did not affect growth of established FTE organoids (mainly secretory cells) in the BET medium, which is consistent with a recent study.[12] In addition, we also found that IWP2 treatment did not significantly affect size and number of organoids from the above-described FTE/stromal cell co-culture (Figure S5D). These data suggest that Wnt signaling is not absolutely required for the maintenance of murine FTE cells, but activation of Wnt signaling can support differentiation of FTE cells toward the ciliated lineage. Consistent with this notion, in a recent *in vivo* study, analysis of Wnt-responsive cells in mouse oviducts supported the requirement of active Wnt signaling in FTE maturation and differentiation during postnatal development.[17] Together, these studies support a role of the FT stromal cells in regulating differentiation of FTE cells, which is consistent with an emerging notion that the stromal niche not only regulates self-renewal of epithelial stem cells, but also supports differentiation of epithelial cells.[18–20]

IGF1 supports FTE organoids

In addition to differentiation-inducing signals from the niche, we also wanted to identify secreted factors from the FT stromal niche that can support proliferation (and survival) of FTE cells. For this purpose, we focused on IGF1, a well-established growth factor that activates IGF/IGF1R signaling. Whereas *Igf1* was only expressed in FT stromal cells (mainly in FT_3 cells), its receptor gene *Igf1r* was expressed in both FTE cells [mainly in FT_4 (secretory) and FT_7 (ciliated) cells] and some stromal cells (Figure 2A). We noticed addition of IGF1 to the BET medium slightly increased the size of organoids formed from freshly sorted $Lin^{-}CD24^{+}$ FTE cells than the control treatment, but the difference did not reach statistical significance (Figure S5E). We reasoned that inclusion of EGF in the BET medium may activate growth-promoting pathways

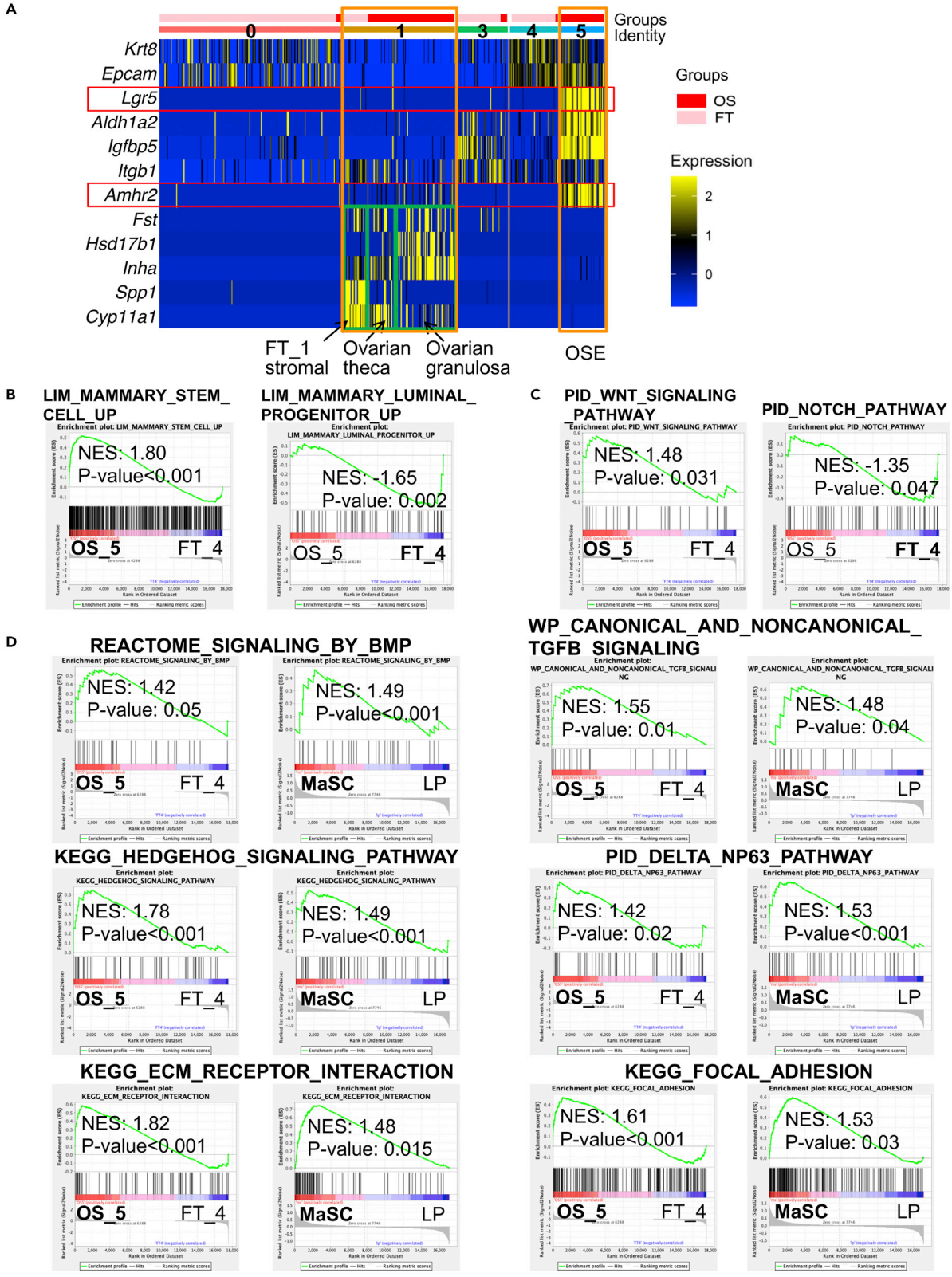
A
0
1
3
4
5
Groups
Identity
Krt8
Epcam
Lgr5
Aldh1a2
Igfbp5
Itgb1
Amhr2
Fst
Hsd17b1
Inha
Spp1
Cyp11a1
Groups
OS
FT
Expression
2
1
0
FT_1 stromal
Ovarian theca
Ovarian granulosa
OSE
B
LIM_MAMMARY_STEM_CELL_UP
NES: 1.80
P-value<0.001
OS_5
FT_4
LIM_MAMMARY_LUMINAL_PROGENITOR_UP
NES: -1.65
P-value: 0.002
OS_5
FT_4
C
PID_WNT_SIGNALING_PATHWAY
NES: 1.48
P-value: 0.031
OS_5
FT_4
PID_NOTCH_PATHWAY
NES: -1.35
P-value: 0.047
OS_5
FT_4
D
REACTOME_SIGNALING_BY_BMP
NES: 1.42
P-value: 0.05
OS_5
FT_4
NES: 1.49
P-value<0.001
MaSC
LP
WP_CANONICAL_AND_NONCANONICAL_TGFB_SIGNALING
NES: 1.55
P-value: 0.01
OS_5
FT_4
NES: 1.48
P-value: 0.04
MaSC
LP
KEGG_HEDGEHOG_SIGNALING_PATHWAY
NES: 1.78
P-value<0.001
OS_5
FT_4
NES: 1.49
P-value<0.001
MaSC
LP
PID_DELTA_NP63_PATHWAY
NES: 1.42
P-value: 0.02
OS_5
FT_4
NES: 1.53
P-value<0.001
MaSC
LP
KEGG_ECM_RECEPTOR_INTERACTION
NES: 1.82
P-value<0.001
OS_5
FT_4
NES: 1.48
P-value: 0.015
MaSC
LP
KEGG_FOCAL_ADHESION
NES: 1.61
P-value<0.001
OS_5
FT_4
NES: 1.53
P-value: 0.03
MaSC
LP

Figure 5. Summary of OS cell clusters

(A) A heatmap showing expression of representative genes in clusters #5 (OSE cells) and #1. Cluster #1 can be further divided into three sub-clusters, including FT_1 stromal cells, ovarian stromal/theca cells, and ovarian granulosa cells.

(B) GSEA showing enrichment of gene sets for MaSCs and mammary LPs in OS_5 OSE cells and FT_4 secretory cells, respectively.

(C) GSEA showing enrichment of gene sets for Wnt signaling and Notch signaling in OS_5 OSE cells and FT_4 secretory cells, respectively.

(D) GSEA showing enrichment of gene sets common for both OS_5 OSE cells (in relation to FT_4 secretory cells) and MaSCs (in relation to mammary LPs). Gene expression data for murine MaSCs and LPs were based on GEO database accession #: GSE19446.

See also Figure S6.

in a way redundant to IGF/IGF1R signaling; we therefore removed EGF from the BET medium (i.e., BT medium) and supplemented it with IGF1 (BT + IGF1). The use of BT + IGF1 medium indeed significantly increased the sizes of organoids formed from the sorted $Lin^{-}CD24^{+}$ FTE cells than those in the BT medium (Figures 4D and 4E). We showed above that co-culture of $Lin^{-}CD24^{+}$ FTE cells with $Lin^{-}CD24^{-}$ stromal cells enhanced their organoid formation (Figures 4A–4C). Because these stromal cells can produce IGF1 (Figure 2A), we treated the co-culture with an IGF1R inhibitor, Picropodophyllin (PPP),[42] and found that this treatment significantly inhibited the FTE organoid growth in a dose-dependent manner (Figures 4F and 4G). This data suggests that the enhancement of FTE organoid growth in the co-culture system is in part because of the IGF/IGF1R signaling.

To study the effect of IGF/IGF1R signaling on the long-term growth of FTE organoid cells, we performed serial passages of established organoids (i.e., enriched with secretory cells) under the BT + IGF1 medium, and compared them to those under the BET or BT medium. We found that in each passage, significantly larger and more organoids were formed under the BT + IGF1 medium or BET medium than the BT medium (Figure 4H), suggesting that similar to EGF, IGF1 is capable of supporting FTE organoid growth long-term as well. Of note, the organoids formed under the BT + IGF1 medium were slightly less in number and size than those under the BET medium (Figures 4H and S5F). This could be because of a potential role of IGF1 in also supporting ciliated cell differentiation, as we observed acetylated tubulin $(AcTUB)^{+}$ organoid cells (i.e., ciliated lineage) under the BT + IGF1 medium, but not the BET medium (Figure S5G).

We also performed a similar serial passage experiment for P0 organoids from the co-culture and observed the same effect of IGF1 in supporting long-term growth of FTE organoids (Figure 4I). In addition, from this experiment, we observed that removal of EGF from the BET medium from this P0 co-culture system (i.e., BT medium plus stromal cells) led to formation of smaller and less organoids than those under the BET medium (with stromal cells, Figure 4I). However, the reduction was not as profound as that observed from the established organoids (i.e., BT vs. BET, without stromal cells; compare Figures 4I–4H, left plots; representative organoid pictures are shown in Figure S5H, compared to S5F). This difference could be because of the presence of stromal cells in the P0 co-culture, which could produce IGF1. Nevertheless, IGF1 produced from the co-cultured stromal cells under the BT medium still did not support organoid growth from primary FTE cells to a level comparable to that stimulated by the exogenously added EGF (BET) or IGF1 (BT + IGF1) (Figure 4I). This can be explained by a possibility that these stromal cells also produce several IGF binding proteins (e.g., IGFBP7, 4, 6, 5, Figure S5I), which can negatively regulate IGF/IGF1R signaling by reducing the local availability of IGF1 to its receptor.[43] Overall, our data support that IGF1 is a secreted factor from the FT stromal niche that can support long-term growth and possibly also differentiation (to ciliated cells) of FTE cells.

OS cell types

In our single cell dataset, cells from the OS tissues were almost exclusively distributed in two clusters, clusters #5 and #1 (Figures 1B–1D). Cluster #5 was composed of cells only from the OS tissues. We found that the majority of OS_5 cells highly expressed *Lgr5* (Figure 5A), suggesting they represent $LGR5^{+}$ OSE stem/progenitor cells described previously,[15,16] and OS_5 is a cluster of OSE cells. Of interest, *Amhr2*, a well-known gene encoding the receptor for the anti-Müllerian hormone and whose control region was utilized to drive Cre expression in the commonly used *Amhr2-Cre* mouse line,[44] was highly expressed in most OS_5 OSE cells as well (Figure 5A). Of note, *Amhr2* is a mesenchymal cell marker gene of the female reproductive tract,[45] suggesting OS_5 OSE cells may have features of mesenchymal cells. About 80% of cells in cluster #1 were also from the OS tissues (Figures 5A and S1D). Of note, in the UMAP plot, these OS_1 cells formed two sub-clusters, with one sub-cluster clustered more closely to cells from the FT and the other sub-cluster only composed of OS cells (Figures 1B and 1C). By comparing to expression signatures of various cell populations in human ovarian cortex defined by scRNA-seq,[46] we found that OS_1 cells exhibited a significant

enrichment of the human ovarian granulosa cell signature (Figure S6A), suggesting a subset of OS_1 cells may represent ovarian granulosa cells. By using select marker genes (e.g., based on The Human Protein Atlas[25]), we could further divide the entire cluster #1 into three sub-clusters, including an ovarian granulosa cell sub-cluster expressing high levels of *Hsd17b1*, *Inha* and *Fst*, an ovarian stromal/theca cell sub-cluster expressing a high level of *Cyp11a1* and intermediate levels of *Inha* and *Fst*, and the FT_1 stromal cell sub-cluster expressing high levels of *Spp1* and *Cyp11a1* (Figure 5A; their locations in the UMAP plot is shown in Figure S6B). Of note, outside of the OS_5 cluster, *Amhr2* was only found expressed in a small number of OS_1 cells, and was almost entirely negative in FT cells (both epithelial and stromal) (Figures 5A and S6C).

Distinct programs in OSE versus FTE cells

Because both OSE cells and FTE cells can serve as cells-of-origin of EOCs, we focused on OSE cells in OS_5. By GSEA, we found that top enriched pathway gene sets in OS_5 cells (compared to the rest of single cells) included those related to complement cascade, sex development, FZD regulation (related to Wnt signaling), and cell adhesion/ECM (Figure S6D).

Recent studies demonstrated that as cells-of-origin of EOCs, OSE and FTE cells exhibited different courses of EOC development and the resulting EOC cells had different drug sensitivities,[12,13] raising a possibility that their intrinsic gene expression programs may contribute to these differences (at least partially). We therefore directly compared transcriptomes of OS_5 OSE cells to those of FT_4 FTE cells. Among gene sets enriched in OS_5 cells, top enriched ones included complement cascade, and ECM/basement membranes/collagens-related (Figure S6E). This expression signature further supports that OSE cells in OS_5 have many features of mesenchymal cells, even though they also express epithelial cell markers (e.g., *Krt8*, *Epcam*, Figure 5A). Among those enriched in FT_4 cells, top enriched ones were mainly those related to metabolism (Figure S6E).

As described above, FT_4 cells exhibited features of mammary LPs (Figures 2A and 2B). Of interest, a direct comparison of OS_5 cells and FT_4 cells not only confirmed enrichment of the mammary LP gene set in FT_4 cells, but also enrichment of the mammary stem cell (MaSC, i.e., basal cell) gene set in OS_5 cells (Figure 5B). In mammary epithelial cells (MECs), Wnt signaling plays an important role in self-renewal of MaSCs/basal MECs,[47–49] whereas Notch signaling plays key roles in specification of MaSCs to luminal MECs and in maintaining luminal cells (mainly LPs).[47,50–52] Consistent with these, we found that gene sets for Wnt and Notch signaling pathways were upregulated in OS_5 OSE and FT_4 FTE cells (Figure 5C), respectively, suggesting differential activities of these two pathways in two different cellular origins of EOCs. Furthermore, in both OSE cells and their MEC-counterpart, MaSCs, in addition to Wnt signaling, gene sets related to BMP signaling, Hedgehog signaling, TGFβ signaling, ΔNp63 pathway, ECM receptor interaction, and focal adhesion were commonly upregulated in both (Figure 5D). Thus, the similarities of these two cell types are attributed to their common pathway activities and mesenchymal-like expression programs. Lastly, in both FTE secretory cells and their MEC-counterpart, mammary LPs, in addition to Notch signaling, metabolism-related gene sets (e.g., glycolysis/gluconeogenesis, pentose phosphate pathway) were commonly upregulated in both as well (Figure S6F). Of note, even though a gene set related to steroid hormone biosynthesis was enriched in FT_4 cells (Figure S6E), this should not be because of the presence of any OS cells in cluster #4, as FT_4 is a subset of this cluster only containing cells from FT tissues (Figure 1D). Overall, we conclude that the intrinsic difference in gene expression programs of OSE versus FTE cells, in a way similar to the difference between MaSCs and mammary LPs, may provide one explanation for different courses of EOC development from them.[12,13]

Similar programs in OSE cells and FT_3 stromal cells

When examining top-enriched genes in each cell cluster (Figure S1E), we noticed that among various cell clusters, cluster #3 (mainly FT_3 stromal cells) was the only cluster that also exhibited expression of many top-enriched genes of cluster #5 (OS_5 OSE cells), and vice versa. This observation raised a possibility that OS_5 OSE cells might more closely resemble FT_3 stromal cells (than FTE cells, e.g., those in FT_4) at the molecular level. In fact, at the pathway level, by GSEA, we found that multiple developmental (e.g., Wnt, Hedgehog/SMO), growth factor (e.g., FGF, IGF) and immune (e.g., complement, antigen processing and presentation) pathway-related gene sets, as well as matrisome/matrisome-associated gene sets, were highly enriched in both OS_5 and FT_3 groups (Figures 6A–6D). This similarity suggests that these two cell types may have shared functional roles.

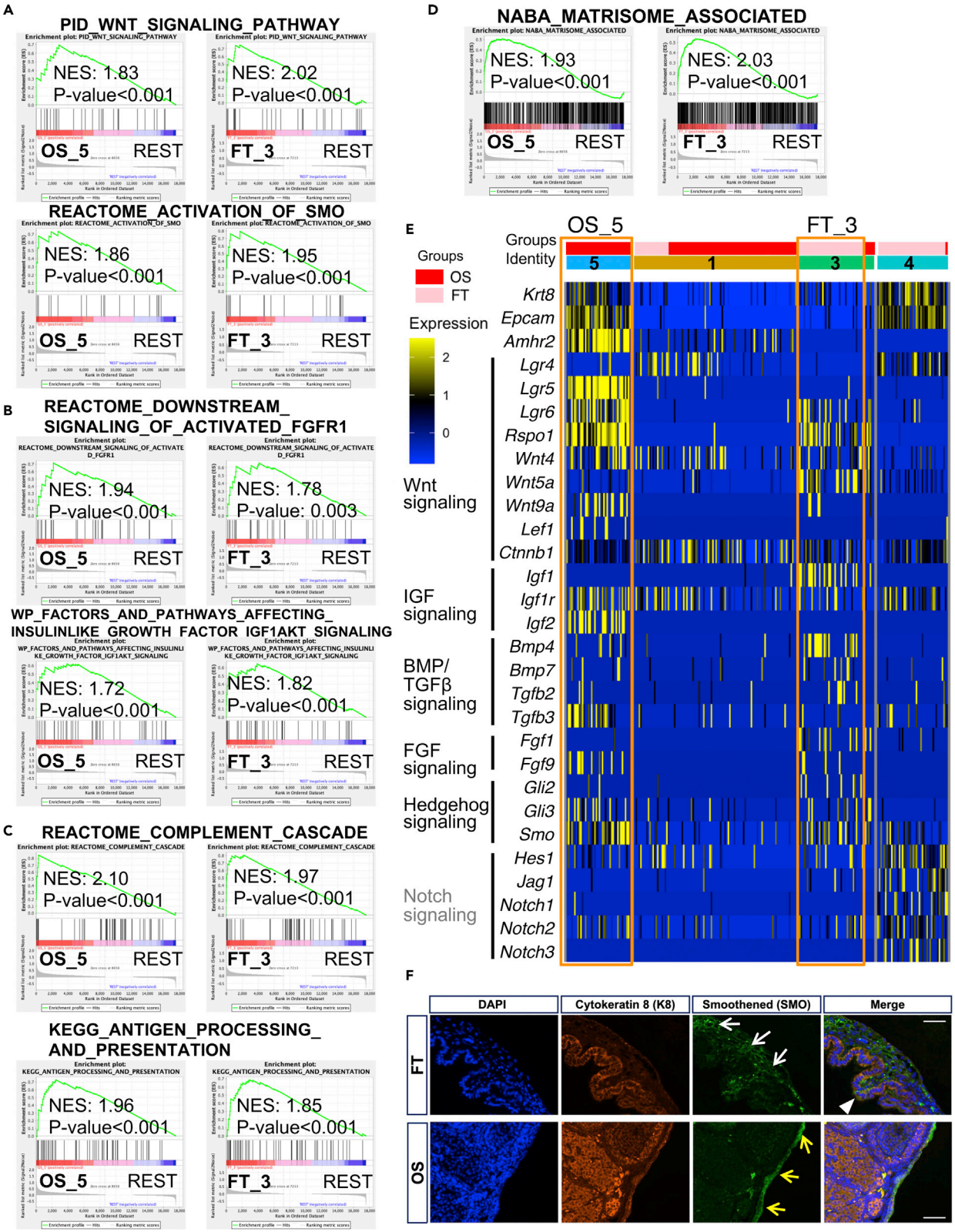
A
PID_WNT_SIGNALING_PATHWAY
NES: 1.83
P-value<0.001
OS_5
REST
NES: 2.02
P-value<0.001
FT_3
REST
REACTOME_ACTIVATION_OF_SMO
NES: 1.86
P-value<0.001
NES: 1.95
P-value<0.001
B
REACTOME_DOWNSTREAM_SIGNALING_OF_ACTIVATED_FGFR1
NES: 1.94
P-value<0.001
NES: 1.78
P-value: 0.003
WP_FACTORS_AND_PATHWAYS_AFFECTING_INSULINLIKE_GROWTH_FACTOR_IGF1AKT_SIGNALING
NES: 1.72
P-value<0.001
NES: 1.82
P-value<0.001
C
REACTOME_COMPLEMENT_CASCADE
NES: 2.10
P-value<0.001
NES: 1.97
P-value<0.001
KEGG_ANTIGEN_PROCESSING_AND_PRESENTATION
NES: 1.96
P-value<0.001
NES: 1.85
P-value<0.001
D
NABA_MATRISOME_ASSOCIATED
NES: 1.93
P-value<0.001
NES: 2.03
P-value<0.001
E
OS_5
FT_3
Groups
Identity
5
1
3
4
Groups
OS
FT
Expression
2
1
0
Krt8
Epcam
Amhr2
Lgr4
Lgr5
Lgr6
Rspo1
Wnt4
Wnt5a
Wnt9a
Lef1
Ctnnb1
Wnt signaling
Igf1
Igf1r
Igf2
IGF signaling
Bmp4
Bmp7
Tgfb2
Tgfb3
BMP/TGFβ signaling
Fgf1
Fgf9
FGF signaling
Gli2
Gli3
Smo
Hedgehog signaling
Hes1
Jag1
Notch1
Notch2
Notch3
Notch signaling
F
DAPI
Cytokeratin 8 (K8)
Smoothened (SMO)
Merge
FT
OS

Figure 6. Similarities in expression programs of OS_5 OSE cells and FT_3 stromal cells

(A–D) GSEA showing developmental pathway (A), growth factor pathway (B), immune pathway (C), and matrisome (D)-related gene sets were significantly enriched in both OS_5 OSE cells and FT_3 stromal cells, when compared to the rest of single cells (from the entire FT + OS dataset).

(E) A heatmap showing genes encoding secreted factors and signaling molecules were expressed in *Lgr5*$^+$ OSE cells in OS_5, with many of such genes exhibiting a similar expression pattern to FT_3 stromal cells (cell clusters highlighted).

(F) Co-immunofluorescence staining of FT and ovary (OS) sections for cytokeratin 8 (K8) and Smoothened (SMO); white and yellow arrows indicate FT stromal cells (K8$^-$) and OSE cells (K8$^+$) positive for Smoothened, white arrowhead indicates rare K8$^+$ FTE cells positive for Smoothened. Scale bars = 50 μm.

See also Figure S7.

OS_5 OSE cells may serve as their now niche

Recent organoid culture study of OSE cells demonstrated their strong dependency on active Wnt signaling.[12] As epithelial stem cell niche often produces R-spondins to support high levels of Wnt signaling activity in epithelial stem cells, we examined "location" of *Rspo* gene expression in OS single cells. We found that *Rspo1* was the only *Rspo* gene expressed and its expression was almost exclusively found in *Lgr5*$^+$ OSE cells in the OS_5 cluster (Figure 6E). This expression pattern raises a possibility that *Lgr5*$^+$ OSE stem/progenitor cells serve as their own niche by producing R-spondin1 as well as other factors. Previously, the hilum region of the mouse ovary was proposed as the stem cell niche for OSE cells.[15] As this region is enriched with LGR5$^+$ OSE cells, our notion that LGR5$^+$ OSE cells may serve as their own niche is not inconsistent with this study.

Matrisome is the ensemble of genes encoding ECM and ECM-associated proteins; the latter includes ECM-affiliated proteins, ECM regulators and secreted factors.[53] The significant enrichment of matrisome-associated gene set (which includes secreted factor genes) in both OS_5 and FT_3 clusters (Figure 6D) raised a possibility that OS_5 OSE cells might exhibit a similarity in their expression of niche secreted factor genes to that in FT_3 stromal cells (which serve as a stromal niche for FTE cells, Figures 2 and 4). In fact, among secreted factors, we found that Wnt signaling-related *Rspo1* and *Wnt4* were expressed in many cells in both clusters; *Bmp4* and *Bmp7*, involved in BMP signaling that supports epithelial differentiation, were also expressed in cells from both clusters (Figure 6E). Although *Igf1* was only expressed in FT_3 stromal cells, *Igf2*, which can also activate IGF/IGF1R signaling,[54] was highly expressed in OS_5 OSE cells, which highly expressed its receptor gene *Igf1r* as well (Figure 6E). A comparison of secreted factors revealed expression of additional factors (either identical or in the same family) in cells from both clusters, such as *Tgfb* (TGFβ signaling), *Fgf* (FGF/FGFR signaling), *S100a10*, *Angptl2*, and *Scube2* (Hedgehog signaling) (Figure S7A). This data further supports that OS_5 OSE cells may serve as their own niche, by producing these secreted factors themselves.

Among developmental pathways upregulated in both OS_5 and FT_3 cells, related to Wnt signaling, we found that although Wnt pathway marker *Lgr5* was only expressed in OSE cells in OS_5, the related LGR factor *Lgr6* was expressed in both OS_5 OSE cells and FT_3 stromal cells (Figure 6E). Related to Hedgehog signaling, in support of its involvement in both clusters, we found that its key receptor (i.e., Smoothened) gene *Smo* and downstream effector genes *Gli2* and *Gli3* (which encode for key transcription factors that mediate Sonic hedgehog signals in the mouse[55]), were expressed in both clusters (Figure 6E). To validate this, we performed co-immunofluorescence staining of FT and ovary sections for Smoothened and the epithelial marker Keratin 8 (K8) (Figure 6F). We found that in the FT, the staining patterns of these two markers were largely mutually exclusive; the majority of the Smoothened signal was observed in K8$^-$ stromal cells and only few K8$^+$ FTE cells were positive for Smoothened. In contrast, in the ovary, K8$^+$ OSE cells were mostly positive for Smoothened. In addition to these two clusters, Hedgehog signaling should also be active in FT_7, which is composed of FT ciliated cells and Hedgehog signaling is active in ciliated cells.[56] In fact, by GSEA, we observed that gene sets related to Hedgehog signaling were enriched not only in OS_5 and FT_3 cells, but also in FT_7 cells (e.g., Figure S7B). However, although top-enriched Hedgehog signaling-related genes were similar in OS_5 and FT_3 cells (e.g., those encoding Hedgehog pathway co-receptors GAS1 and CDON, as well as the key transmembrane signaling protein SMO), they were different in FT_7 cells (Figure S7B), raising a possibility that the Hedgehog signaling activity in OS_5 and FT_3 cells may be related to its role in niche regulation,[20] whereas the Hedgehog pathway in FT_7 cells is related to its role in ciliated cell biology.[56]

DISCUSSION

Our integrated single cell expression analysis of FT and OS tissues has revealed three important cell populations related to EOC initiation and development, including FTE secretory cells in FT_4, FT stromal cells

in FT_3, and OSE cells in OS_5. Both FT_4 FTE cells and OS_5 OSE cells are enriched with their corresponding stem/progenitor cell populations and may serve as cells-of-origin of EOCs. We provided experimental evidence to support that the FT stromal cells may serve as a niche for FTE cells, by regulating both differentiation (toward the ciliated cell lineage) and proliferation/survival of FTE cells (particularly ciliated cells). We showed that even though both FTE and OSE cells can serve as cells-of-origin of EOCs, their intrinsic lineage-specific expression programs are very different. In contrast, OSE cells exhibit an intriguing similarity (in terms of niche factor expression and pathway activities) to FT_3 stromal cells at the molecular level, raising a possibility that these *Lgr5*$^{+}$ OSE cells may be largely regulated by themselves (as their own niche).

Another interesting observation from our scRNA-seq analysis is the shared gene expression programs between FTE secretory cells in FT_4 and mammary LPs, as well as between OSE cells in OS_5 and MaSCs (basal MECs), respectively. Similar to the debate on the cellular origin of EOC, the cellular origin of breast cancer, particularly basal-like breast cancer (BLBC), has also been a topic of long-standing debate. Because of the basal differentiation nature of BLBC, the classic view is that BLBC is derived from transformation of MECs in the basal lineage, which possess the multipotent MaSC activity.[57,58] However, more recent studies, largely based on *BRCA1*-associated BLBC, suggested that cells-of-origin of BLBC are in the luminal lineage, specifically, mammary LPs.[59–61] Nevertheless, at least in experimental models, it has been shown that both basal and luminal MECs could serve as cellular origins of mammary tumors with diverse phenotypes.[62–64] Developmentally, both basal MECs/MaSCs and luminal MECs/LPs are derived from common fetal MaSCs (fMaSCs).[65–67] Of note, even though OSE and FTE cells are from two different organs, they also have a common ancestor. OSE cells are mesothelial cells, whereas FTE cells are Müllerian duct-derived epithelial cells, and both are developed from the coelomic epithelium of the early embryo.[68] Our single cell data suggests that: (1) similar developmental programs may be utilized to generate adult cell types in these two systems from their corresponding common ancestors; (2) cancer development in these two systems from distinct cellular origins (e.g., basal versus luminal MECs, OSE versus FTE cells) may on one hand, converge to the cell state of their common embryonic origin, but on the other hand, also partially retain their original (adult) identity. Of interest, genomic studies of HGSOCs and BLBCs revealed many molecular commonalities of these two diverse cancer types (e.g., both associated with *BRCA1* mutation).[69] The similarity in expression profiling of FT_4 cells and mammary LPs not only supports that FTE cells in this cluster may represent FTE stem/progenitor cells to serve as the cellular origin of HGSOCs, but also provides an explanation for the molecular similarities of these two cancer types.

An emerging theme of the epithelial stem cell niche is that it not only maintains the stemness of an epithelial stem cell, but also contributes factors (e.g., BMPs) required for stem cell differentiation, and the latter is orchestrated by Hedgehog signaling activity in the niche.[20] The expression patterns of Hedgehog signaling-related genes described above (Figures 6E, 6F, and S7B) suggest that the Hedgehog pathway is involved in both OS_5 and FT_3 cells and the activity of this pathway may be related to their roles in niche regulation. In the mammary gland, it was shown that the Hedgehog pathway activity in mammary stromal cells regulates stromal *Esr1* expression, and that the activity of its downstream effector Gli2 coordinates a hormone-responsive niche signaling program for MaSCs.[70] Our single cell data suggests that in the FT and OS tissues, Hedgehog signaling may play a similar role in regulating expression of secreted factors and *Esr1* in FT stromal cells and OSE cells, which may serve as niches to regulate self-renewal and differentiation of FTE and OSE stem/progenitor cells, respectively. In support of this, it has been reported that constitutive activation of Hedgehog signaling in the mesenchyme of Müllerian duct led to increased expression of niche factors (e.g., *Wnt4* and *Wnt5a*) in the FT and aberrant development of the reproductive tract.[71] Of note, estrogen exposure is a risk factor for EOC.[32] The concept of the hormone-responsive niche described here may help understand how estrogen exposure may increase the potential of developing EOC, possibly via perturbing regulation of FTE or OSE stem/progenitor cells by their corresponding niches.

Recent comprehensive whole-exome sequence and copy number analyses of laser capture microdissected FT lesions (i.e., p53 signatures, STICs, and FT carcinomas), EOCs, and metastases from the same individuals demonstrated the lineage continuity between FTE cells and ovarian tumors.[72] A multi-center integrated genomic analysis of advanced stage ovarian tumors also showed that HGSOCs with and without associated STICs had molecular profiles more similar to normal FTE cells than OSE cells.[73] Although these comprehensive genomic studies do not rule out the possibility of an OSE origin for some EOCs, both clinical and mouse modeling studies strongly support the FTE origin for HGSOCs.[74] The difference in niche organizations of FTE and OSE cells may provide mechanistic insights into why FTE cells are the preferred origin of

HGSOCs. It may also provide an explanation for the recently observed shorter latency and higher penetrance of development of HGSOCs from FTE cells than OSE cells.[12,13] FTE cells, on acquisition of initiating oncogenic events, may on one hand, become independent from their stromal niche-mediated growth/survival support, on the other hand, also escape their stromal niche-induced differentiation (Figure S7C). In contrast, if OSE cells are largely regulated by their own niche, even on acquisition of the same initiating oncogenic events, they may be still under the regulation of differentiation-inducing signals from themselves (e.g., BMP/TGFβ pathways, Figure 5D), which may explain why they are more resistant to transformation than FTE cells (Figure S7C). Further studies are warranted to test these possibilities.

Limitations of the study

Because of the small number of single cells in our dataset, only major epithelial and stromal cell populations in FT and OS tissues were studied. We did not investigate other cell types (e.g., immune cells, endothelial cells) in these two organs. In addition, we also cannot rule out the existence of rare epithelial and stromal cell populations in them. In the co-culture experiment, because of a technical difficulty, we only presented data from the co-culture of FTE cells with $Lin^{-}CD24^{-}$ FT stromal cells. We have not definitively demonstrated whether it is the $CD140a^{+}$ subset of the FT stromal cells that serves as the niche to support homeostasis of FTE cells.

STAR★METHODS

Detailed methods are provided in the online version of this paper and include the following:

- KEY RESOURCES TABLE
- RESOURCE AVAILABILITY
  - Lead contact
  - Materials availability
  - Data and code availability
- EXPERIMENTAL MODEL AND SUBJECT DETAILS
  - Mouse lines
- METHOD DETAILS
  - Mouse FT and OS sample preparation for scRNA-seq
  - Generation of single-cell cDNA libraries and sequencing
  - scRNA-seq data analysis
  - Flow cytometry
  - Organoid culture and co-culture
  - Immunofluorescence
  - RNA quantification and real-time PCR
- QUANTIFICATION AND STATISTICAL ANALYSIS

SUPPLEMENTAL INFORMATION

Supplemental information can be found online at https://doi.org/10.1016/j.isci.2022.105861.

ACKNOWLEDGMENTS

The authors would like to thank the Harvard Chan Bioinformatics Core, Harvard T.H. Chan School of Public Health, Boston, MA for assistance with processing the scRNA-seq raw sequencing data, as well as Sarah Boswell and Alex Ratner at ICCB-L Single Cell Core, Harvard Medical School, Boston, MA for consulting on this scRNA-seq project and for inDrop-based cell encapsulation. Diagrams in Figure 1A, Figure S7C, and Graphical Abstract were created with BioRender.com. This research was supported by a U.S. Department of Defense Ovarian Cancer Research Program Pilot Award (W81XWH-14-1-0280), a Cancer Program Pilot Grant from Harvard Stem Cell Institute (DP-0164-17-00), and Sundry Fund from Brigham and Women's Hospital (BWH) to ZL.

AUTHOR CONTRIBUTIONS

Z.L. and E.S.P. perceived the conceptual ideas and designed the experiments. G.Q., E.S.P., X.C., S.H., D.X., F.R., and G.L. performed the experiments. G.Q., H.C., G.C.Y., and Z.L. analyzed the scRNA-seq data. G.Q., E.S.P., X.C., and Z.L. wrote the manuscript.

DECLARATION OF INTERESTS

The authors declare no competing interests.

INCLUSION AND DIVERSITY

We support inclusive, diverse, and equitable conduct of research.

Received: March 15, 2022
Revised: November 17, 2022
Accepted: November 18, 2022
Published: January 20, 2023

REFERENCES

1. Quartuccio, S.M., Lantvit, D.D., Bosland, M.C., and Burdette, J.E. (2013). Conditional inactivation of p53 in mouse ovarian surface epithelium does not alter MIS driven smad2-dominant negative epithelium-lined inclusion cysts or teratomas. PLoS One *8*, e65067. https://doi.org/10.1371/journal.pone.0065067.

2. Lheureux, S., Gourley, C., Vergote, I., and Oza, A.M. (2019). Epithelial ovarian cancer. Lancet *393*, 1240–1253. https://doi.org/10.1016/S0140-6736(18)32552-2.

3. Bast, R.C., Jr., Hennessy, B., and Mills, G.B. (2009). The biology of ovarian cancer: new opportunities for translation. Nat. Rev. Cancer *9*, 415–428. https://doi.org/10.1038/nrc2644.

4. Lisio, M.A., Fu, L., Goyeneche, A., Gao, Z.H., and Telleria, C. (2019). High-grade serous ovarian cancer: basic sciences, clinical and therapeutic standpoints. Int. J. Mol. Sci. *20*, 952. https://doi.org/10.3390/ijms20040952.

5. Kurman, R.J., and Shih, I.M. (2016). The dualistic model of ovarian carcinogenesis: revisited, revised, and expanded. Am. J. Pathol. *186*, 733–747. https://doi.org/10.1016/j.ajpath.2015.11.011.

6. Chene, G., Dauplat, J., Radosevic-Robin, N., Cayre, A., and Penault-Llorca, F. (2013). Tu-be or not tu-be: that is the question. about serous ovarian carcinogenesis. Crit. Rev. Oncol. Hematol. *88*, 134–143. https://doi.org/10.1016/j.critrevonc.2013.03.004.

7. Kessler, M., Fotopoulou, C., and Meyer, T. (2013). The molecular fingerprint of high grade serous ovarian cancer reflects its fallopian tube origin. Int. J. Mol. Sci. *14*, 6571–6596. https://doi.org/10.3390/ijms14046571.

8. Kuhn, E., Kurman, R.J., Vang, R., Sehdev, A.S., Han, G., Soslow, R., Wang, T.L., and Shih, I.M. (2012). TP53 mutations in serous tubal intraepithelial carcinoma and concurrent pelvic high-grade serous carcinoma–evidence supporting the clonal relationship of the two lesions. J. Pathol. *226*, 421–426. https://doi.org/10.1002/path.3023.

9. Perets, R., Wyant, G.A., Muto, K.W., Bijron, J.G., Poole, B.B., Chin, K.T., Chen, J.Y.H., Ohman, A.W., Stepule, C.D., Kwak, S., et al. (2013). Transformation of the fallopian tube secretory epithelium leads to high-grade serous ovarian cancer in Brca;Tp53;Pten models. Cancer Cell *24*, 751–765. https://doi.org/10.1016/j.ccr.2013.10.013.

10. Sherman-Baust, C.A., Kuhn, E., Valle, B.L., Shih, I.M., Kurman, R.J., Wang, T.L., Amano, T., Ko, M.S.H., Miyoshi, I., Araki, Y., et al. (2014). A genetically engineered ovarian cancer mouse model based on fallopian tube transformation mimics human high-grade serous carcinoma development. J. Pathol. *233*, 228–237. https://doi.org/10.1002/path.4353.

11. Wu, R., Zhai, Y., Kuick, R., Karnezis, A.N., Garcia, P., Naseem, A., Hu, T.C., Fearon, E.R., and Cho, K.R. (2016). Impact of oviductal versus ovarian epithelial cell of origin on ovarian endometrioid carcinoma phenotype in the mouse. J. Pathol. *240*, 341–351. https://doi.org/10.1002/path.4783.

12. Lõhmussaar, K., Kopper, O., Korving, J., Begthel, H., Vreuls, C.P.H., van Es, J.H., and Clevers, H. (2020). Assessing the origin of high-grade serous ovarian cancer using CRISPR-modification of mouse organoids. Nat. Commun. *11*, 2660. https://doi.org/10.1038/s41467-020-16432-0.

13. Zhang, S., Dolgalev, I., Zhang, T., Ran, H., Levine, D.A., and Neel, B.G. (2019). Both fallopian tube and ovarian surface epithelium are cells-of-origin for high-grade serous ovarian carcinoma. Nat. Commun. *10*, 5367. https://doi.org/10.1038/s41467-019-13116-2.

14. Visvader, J.E. (2011). Cells of origin in cancer. Nature *469*, 314–322. https://doi.org/10.1038/nature09781.

15. Flesken-Nikitin, A., Hwang, C.I., Cheng, C.Y., Michurina, T.V., Enikolopov, G., and Nikitin, A.Y. (2013). Ovarian surface epithelium at the junction area contains a cancer-prone stem cell niche. Nature *495*, 241–245. https://doi.org/10.1038/nature11979.

16. Ng, A., Tan, S., Singh, G., Rizk, P., Swathi, Y., Tan, T.Z., Huang, R.Y.J., Leushacke, M., and Barker, N. (2014). Lgr5 marks stem/progenitor cells in ovary and tubal epithelia. Nat. Cell Biol. *16*, 745–757. https://doi.org/10.1038/ncb3000.

17. Ghosh, A., Syed, S.M., and Tanwar, P.S. (2017). In vivo genetic cell lineage tracing reveals that oviductal secretory cells self-renew and give rise to ciliated cells. Development *144*, 3031–3041. https://doi.org/10.1242/dev.149989.

18. Cai, C., Yu, Q.C., Jiang, W., Liu, W., Song, W., Yu, H., Zhang, L., Yang, Y., and Zeng, Y.A. (2014). R-spondin1 is a novel hormone mediator for mammary stem cell self-renewal. Genes Dev. *28*, 2205–2218. https://doi.org/10.1101/gad.245142.114.

19. Chacón-Martínez, C.A., Koester, J., and Wickström, S.A. (2018). Signaling in the stem cell niche: regulating cell fate, function and plasticity. Development *145*, dev165399. https://doi.org/10.1242/dev.165399.

20. Roberts, K.J., Kershner, A.M., and Beachy, P.A. (2017). The stromal niche for epithelial stem cells: atemplate for regeneration and a brake on malignancy. Cancer Cell *32*, 404–410. https://doi.org/10.1016/j.ccell.2017.08.007.

21. Johnson, P.A., and Giles, J.R. (2013). The hen as a model of ovarian cancer. Nat. Rev. Cancer *13*, 432–436. https://doi.org/10.1038/nrc3535.

22. Morin, P.J., and Weeraratna, A.T. (2016). Genetically-defined ovarian cancer mouse models. J. Pathol. *238*, 180–184. https://doi.org/10.1002/path.4663.

23. Klein, A.M., Mazutis, L., Akartuna, I., Tallapragada, N., Veres, A., Li, V., Peshkin, L., Weitz, D.A., and Kirschner, M.W. (2015). Droplet barcoding for single-cell transcriptomics applied to embryonic stem cells. Cell *161*, 1187–1201. https://doi.org/10.1016/j.cell.2015.04.044.

24. Butler, A., Hoffman, P., Smibert, P., Papalexi, E., and Satija, R. (2018). Integrating single-cell transcriptomic data across different conditions, technologies, and species. Nat. Biotechnol. *36*, 411–420. https://doi.org/10.1038/nbt.4096.

25. The Human Protein Atlas. https://www.proteinatlas.org/.

26. Subramanian, A., Tamayo, P., Mootha, V.K., Mukherjee, S., Ebert, B.L., Gillette, M.A., Paulovich, A., Pomeroy, S.L., Golub, T.R., Lander, E.S., and Mesirov, J.P. (2005). Gene set enrichment analysis: a knowledge-based approach for interpreting genome-wide expression profiles. Proc. Natl. Acad. Sci. USA *102*, 15545–15550.

27. Dinh, H.Q., Lin, X., Abbasi, F., Nameki, R., Haro, M., Olingy, C.E., Chang, H., Hernandez, L., Gayther, S.A., Wright, K.N., et al. (2021).

Single-cell transcriptomics identifies gene expression networks driving differentiation and tumorigenesis in the human fallopian tube. Cell Rep. *35*, 108978. https://doi.org/10.1016/j.celrep.2021.108978.

28. Hu, Z., Artibani, M., Alsaadi, A., Wietek, N., Morotti, M., Shi, T., Zhong, Z., Santana Gonzalez, L., El-Sahhar, S., KaramiNejadRanjbar, M., et al. (2020). The repertoire of serous ovarian cancer non-genetic heterogeneity revealed by single-cell sequencing of normal fallopian tube epithelial cells. Cancer Cell *37*, 226–242.e7. https://doi.org/10.1016/j.ccell.2020.01.003.

29. Lim, E., Wu, D., Pal, B., Bouras, T., Asselin-Labat, M.L., Vaillant, F., Yagita, H., Lindeman, G.J., Smyth, G.K., and Visvader, J.E. (2010). Transcriptome analyses of mouse and human mammary cell subpopulations reveal multiple conserved genes and pathways. Breast Cancer Res. *12*, R21. https://doi.org/10.1186/bcr2560.

30. Ford, M.J., Harwalkar, K., Pacis, A.S., Maunsell, H., Wang, Y.C., Badescu, D., Teng, K., Yamanaka, N., Bouchard, M., Ragoussis, J., and Yamanaka, Y. (2021). Oviduct epithelial cells constitute two developmentally distinct lineages that are spatially separated along the distal-proximal axis. Cell Rep. *36*, 109677. https://doi.org/10.1016/j.celrep.2021.109677.

31. de Lau, W., Peng, W.C., Gros, P., and Clevers, H. (2014). The R-spondin/Lgr5/Rnf43 module: regulator of Wnt signal strength. Genes Dev. *28*, 305–316. https://doi.org/10.1101/gad.235473.113.

32. Nagendra, P.B., Goad, J., Nielsen, S., Rassam, L., Lombard, J.M., Nahar, P., and Tanwar, P.S. (2016). Ovarian hormones through Wnt signalling regulate the growth of human and mouse ovarian cancer initiating lesions. Oncotarget *7*, 64836–64853. https://doi.org/10.18632/oncotarget.11711.

33. Greicius, G., Kabiri, Z., Sigmundsson, K., Liang, C., Bunte, R., Singh, M.K., and Virshup, D.M. (2018). PDGFRalpha(+) pericryptal stromal cells are the critical source of Wnts and RSPO3 for murine intestinal stem cells in vivo. Proc. Natl. Acad. Sci. USA *115*, E3173–E3181. https://doi.org/10.1073/pnas.1713510115.

34. Kabiri, Z., Greicius, G., Madan, B., Biechele, S., Zhong, Z., Zaribafzadeh, H., Edison, Aliyev, J., Aliyev, J., Wu, Y., Bunte, R., et al. (2014). Stroma provides an intestinal stem cell niche in the absence of epithelial Wnts. Development *141*, 2206–2215. https://doi.org/10.1242/dev.104976.

35. Nabhan, A.N., Brownfield, D.G., Harbury, P.B., Krasnow, M.A., and Desai, T.J. (2018). Single-cell Wnt signaling niches maintain stemness of alveolar type 2 cells. Science *359*, 1118–1123. https://doi.org/10.1126/science.aam6603.

36. Sigal, M., Logan, C.Y., Kapalczynska, M., Mollenkopf, H.J., Berger, H., Wiedenmann, B., Nusse, R., Amieva, M.R., and Meyer, T.F. (2017). Stromal R-spondin orchestrates gastric epithelial stem cells and gland homeostasis. Nature *548*, 451–455. https://doi.org/10.1038/nature23642.

37. Ulrich, N.D., Shen, Y.C., Ma, Q., Yang, K., Hannum, D.F., Jones, A., Machlin, J., Randolph, J.F., Jr., Smith, Y.R., Schon, S.B., et al. (2022). Cellular heterogeneity of human fallopian tubes in normal and hydrosalpinx disease states identified using scRNA-seq. Dev. Cell *57*, 914–929.e7. https://doi.org/10.1016/j.devcel.2022.02.017.

38. Roesch, K., Jadhav, A.P., Trimarchi, J.M., Stadler, M.B., Roska, B., Sun, B.B., and Cepko, C.L. (2008). The transcriptome of retinal Muller glial cells. J. Comp. Neurol. *509*, 225–238. https://doi.org/10.1002/cne.21730.

39. Srinivas, S., Watanabe, T., Lin, C.S., William, C.M., Tanabe, Y., Jessell, T.M., and Costantini, F. (2001). Cre reporter strains produced by targeted insertion of EYFP and ECFP into the ROSA26 locus. BMC Dev. Biol. *1*, 4.

40. Xie, Y., Park, E.S., Xiang, D., and Li, Z. (2018). Long-term organoid culture reveals enrichment of organoid-forming epithelial cells in the fimbrial portion of mouse fallopian tube. Stem Cell Res. *32*, 51–60. https://doi.org/10.1016/j.scr.2018.08.021.

41. Langton, P.F., Kakugawa, S., and Vincent, J.P. (2016). Making, exporting, and modulating wnts. Trends Cell Biol. *26*, 756–765. https://doi.org/10.1016/j.tcb.2016.05.011.

42. Klusmann, J.H., Godinho, F.J., Heitmann, K., Maroz, A., Koch, M.L., Reinhardt, D., Orkin, S.H., and Li, Z. (2010). Developmental stage-specific interplay of GATA1 and IGF signaling in fetal megakaryopoiesis and leukemogenesis. Genes Dev. *24*, 1659–1672. https://doi.org/10.1101/gad.1903410.

43. Allard, J.B., and Duan, C. (2018). IGF-binding proteins: why do they exist and why are there so many? Front. Endocrinol. *9*, 117. https://doi.org/10.3389/fendo.2018.00117.

44. Jamin, S.P., Arango, N.A., Mishina, Y., Hanks, M.C., and Behringer, R.R. (2002). Requirement of Bmpr1a for Mullerian duct regression during male sexual development. Nat. Genet. *32*, 408–410. https://doi.org/10.1038/ng1003.

45. Ghosh, A., Syed, S.M., Kumar, M., Carpenter, T.J., Teixeira, J.M., Houairia, N., Negi, S., and Tanwar, P.S. (2020). In vivo cell fate tracing provides No evidence for mesenchymal to epithelial transition in adult fallopian tube and uterus. Cell Rep. *31*, 107631. https://doi.org/10.1016/j.celrep.2020.107631.

46. Wagner, M., Yoshihara, M., Douagi, I., Damdimopoulos, A., Panula, S., Petropoulos, S., Lu, H., Pettersson, K., Palm, K., Katayama, S., et al. (2020). Single-cell analysis of human ovarian cortex identifies distinct cell populations but no oogonial stem cells. Nat. Commun. *11*, 1147. https://doi.org/10.1038/s41467-020-14936-3.

47. Gu, B., Watanabe, K., Sun, P., Fallahi, M., and Dai, X. (2013). Chromatin effector Pygo2 mediates Wnt-notch crosstalk to suppress luminal/alveolar potential of mammary stem and basal cells. Cell Stem Cell *13*, 48–61. https://doi.org/10.1016/j.stem.2013.04.012.

48. van Amerongen, R., Bowman, A.N., and Nusse, R. (2012). Developmental stage and time dictate the fate of Wnt/beta-catenin-responsive stem cells in the mammary gland. Cell Stem Cell *11*, 387–400. https://doi.org/10.1016/j.stem.2012.05.023.

49. Zeng, Y.A., and Nusse, R. (2010). Wnt proteins are self-renewal factors for mammary stem cells and promote their long-term expansion in culture. Cell Stem Cell *6*, 568–577. https://doi.org/10.1016/j.stem.2010.03.020.

50. Bouras, T., Pal, B., Vaillant, F., Harburg, G., Asselin-Labat, M.L., Oakes, S.R., Lindeman, G.J., and Visvader, J.E. (2008). Notch signaling regulates mammary stem cell function and luminal cell-fate commitment. Cell Stem Cell *3*, 429–441.

51. Lafkas, D., Rodilla, V., Huyghe, M., Mourao, L., Kiaris, H., and Fre, S. (2013). Notch3 marks clonogenic mammary luminal progenitor cells in vivo. J. Cell Biol. *203*, 47–56. https://doi.org/10.1083/jcb.201307046.

52. Xu, K., Usary, J., Kousis, P.C., Prat, A., Wang, D.Y., Adams, J.R., Wang, W., Loch, A.J., Deng, T., Zhao, W., et al. (2012). Lunatic fringe deficiency cooperates with the met/caveolin gene amplicon to induce basal-like breast cancer. Cancer Cell *21*, 626–641. https://doi.org/10.1016/j.ccr.2012.03.041.

53. Naba, A., Clauser, K.R., Ding, H., Whittaker, C.A., Carr, S.A., and Hynes, R.O. (2016). The extracellular matrix: tools and insights for the "omics" era. Matrix Biol. *49*, 10–24. https://doi.org/10.1016/j.matbio.2015.06.003.

54. Pollak, M. (2008). Insulin and insulin-like growth factor signalling in neoplasia. Nat. Rev. Cancer *8*, 915–928.

55. Pan, Y., Bai, C.B., Joyner, A.L., and Wang, B. (2006). Sonic hedgehog signaling regulates Gli2 transcriptional activity by suppressing its processing and degradation. Mol. Cell Biol. *26*, 3365–3377. https://doi.org/10.1128/MCB.26.9.3365-3377.2006.

56. Wheway, G., Nazlamova, L., and Hancock, J.T. (2018). Signaling through the primary cilium. Front. Cell Dev. Biol. *6*, 8. https://doi.org/10.3389/fcell.2018.00008.

57. Foulkes, W.D. (2004). BRCA1 functions as a breast stem cell regulator. J. Med. Genet. *41*, 1–5.

58. Liu, S., Ginestier, C., Charafe-Jauffret, E., Foco, H., Kleer, C.G., Merajver, S.D., Dontu, G., and Wicha, M.S. (2008). BRCA1 regulates human mammary stem/progenitor cell fate. Proc. Natl. Acad. Sci. USA *105*, 1680–1685. https://doi.org/10.1073/pnas.0711613105.

59. Lim, E., Vaillant, F., Wu, D., Forrest, N.C., Pal, B., Hart, A.H., Asselin-Labat, M.L., Gyorki, D.E., Ward, T., Partanen, A., et al. (2009). Aberrant luminal progenitors as the candidate target population for basal tumor development in BRCA1 mutation carriers. Nat. Med. *15*, 907–913. https://doi.org/10.1038/nm.2000.

60. Proia, T.A., Keller, P.J., Gupta, P.B., Klebba, I., Jones, A.D., Sedic, M., Gilmore, H., Tung, N., Naber, S.P., Schnitt, S., et al. (2011). Genetic predisposition directs breast cancer phenotype by dictating progenitor cell fate. Cell Stem Cell *8*, 149–163. https://doi.org/10.1016/j.stem.2010.12.007.

61. Molyneux, G., Geyer, F.C., Magnay, F.A., McCarthy, A., Kendrick, H., Natrajan, R., Mackay, A., Grigoriadis, A., Tutt, A., Ashworth, A., et al. (2010). BRCA1 basal-like breast cancers originate from luminal epithelial progenitors and not from basal stem cells. Cell Stem Cell *7*, 403–417. https://doi.org/10.1016/j.stem.2010.07.010.

62. Koren, S., Reavie, L., Couto, J.P., De Silva, D., Stadler, M.B., Roloff, T., Britschgi, A., Eichlisberger, T., Kohler, H., Aina, O., et al. (2015). PIK3CA induces multipotency and multi-lineage mammary tumours. Nature *525*, 114–118. https://doi.org/10.1038/nature14669.

63. Nguyen, L.V., Pellacani, D., Lefort, S., Kannan, N., Osako, T., Makarem, M., Cox, C.L., Kennedy, W., Beer, P., Carles, A., et al. (2015). Barcoding reveals complex clonal dynamics of de novo transformed human mammary cells. Nature *528*, 267–271. https://doi.org/10.1038/nature15742.

64. Van Keymeulen, A., Lee, M.Y., Ousset, M., Brohée, S., Rorive, S., Giraddi, R.R., Wuidart, A., Bouvencourt, G., Dubois, C., Salmon, I., et al. (2015). Reactivation of multipotency by oncogenic PIK3CA induces breast tumour heterogeneity. Nature *525*, 119–123. https://doi.org/10.1038/nature14665.

65. Lilja, A.M., Rodilla, V., Huyghe, M., Hannezo, E., Landragin, C., Renaud, O., Leroy, O., Rulands, S., Simons, B.D., and Fre, S. (2018). Clonal analysis of Notch1-expressing cells reveals the existence of unipotent stem cells that retain long-term plasticity in the embryonic mammary gland. Nat. Cell Biol. *20*, 677–687. https://doi.org/10.1038/s41556-018-0108-1.

66. Spike, B.T., Engle, D.D., Lin, J.C., Cheung, S.K., La, J., and Wahl, G.M. (2012). A mammary stem cell population identified and characterized in late embryogenesis reveals similarities to human breast cancer. Cell Stem Cell *10*, 183–197. https://doi.org/10.1016/j.stem.2011.12.018.

67. Wuidart, A., Sifrim, A., Fioramonti, M., Matsumura, S., Brisebarre, A., Brown, D., Centonze, A., Dannau, A., Dubois, C., Van Keymeulen, A., et al. (2018). Early lineage segregation of multipotent embryonic mammary gland progenitors. Nat. Cell Biol. *20*, 666–676. https://doi.org/10.1038/s41556-018-0095-2.

68. Auersperg, N. (2011). The origin of ovarian carcinomas: a unifying hypothesis. Int. J. Gynecol. Pathol. *30*, 12–21. https://doi.org/10.1097/PGP.0b013e3181f45f3e.

69. Cancer Genome Atlas Network (2012). Comprehensive molecular portraits of human breast tumours. Nature *490*, 61–70. https://doi.org/10.1038/nature11412.

70. Zhao, C., Cai, S., Shin, K., Lim, A., Kalisky, T., Lu, W.J., Clarke, M.F., and Beachy, P.A. (2017). Stromal Gli2 activity coordinates a niche signaling program for mammary epithelial stem cells. Science *356*, eaal3485. https://doi.org/10.1126/science.aal3485.

71. Migone, F.F., Ren, Y., Cowan, R.G., Harman, R.M., Nikitin, A.Y., and Quirk, S.M. (2012). Dominant activation of the hedgehog signaling pathway alters development of the female reproductive tract. Genesis *50*, 28–40. https://doi.org/10.1002/dvg.20786.

72. Labidi-Galy, S.I., Papp, E., Hallberg, D., Niknafs, N., Adleff, V., Noe, M., Bhattacharya, R., Novak, M., Jones, S., Phallen, J., et al. (2017). High grade serous ovarian carcinomas originate in the fallopian tube. Nat. Commun. *8*, 1093. https://doi.org/10.1038/s41467-017-00962-1.

73. Ducie, J., Dao, F., Considine, M., Olvera, N., Shaw, P.A., Kurman, R.J., Shih, I.M., Soslow, R.A., Cope, L., and Levine, D.A. (2017). Molecular analysis of high-grade serous ovarian carcinoma with and without associated serous tubal intra-epithelial carcinoma. Nat. Commun. *8*, 990. https://doi.org/10.1038/s41467-017-01217-9.

74. Bowtell, D.D., Böhm, S., Ahmed, A.A., Aspuria, P.J., Bast, R.C., Jr., Beral, V., Berek, J.S., Birrer, M.J., Blagden, S., Bookman, M.A., et al. (2015). Rethinking ovarian cancer II: reducing mortality from high-grade serous ovarian cancer. Nat. Rev. Cancer *15*, 668–679. https://doi.org/10.1038/nrc4019.

STAR★METHODS

KEY RESOURCES TABLE

REAGENT or RESOURCE	SOURCE	IDENTIFIER
Antibodies		
Alexa Fluor® 700 Rat Anti-Mouse CD24	BD Biosciences	564237; RRID: AB_2738691
CD24 Monoclonal Antibody (M1/69), Biotin	eBioscience	13-0242-82; RRID: AB_466397
PerCP Streptavidin	BD Biosciences	554064
APC/Fire™ 750 anti-mouse CD66a (CEACAM1a)	Biolegend	134519; RRID: AB_2632806
FITC anti-mouse CD66a (CEACAM1a) Antibody	Biolegend	134517; RRID: AB_2632804
CD140a (PDGFRA) Monoclonal Antibody (APA5), PE-Cyanine7	eBioscience	25-1401-80; RRID: AB_2573399
CD61 (Integrin beta 3) Monoclonal Antibody (2C9.G3), PE	eBioscience	12-0611-83; RRID: AB_465719
Biotinylated CD31 (PECAM-1) Monoclonal Antibody (390)	eBioscience	13-0311-85; RRID: AB_466421
Biotinylated CD45 Monoclonal Antibody (30-F11)	eBioscience	13-0451-81; RRID: AB_466445
Biotinylated TER-119 Monoclonal Antibody (TER-119)	eBioscience	13-5921-85; RRID: AB_466798
CD31 (PECAM-1) Monoclonal Antibody (390), APC	eBioscience	17-0311-82; RRID: AB_657735
CD45 Monoclonal Antibody (30-F11), APC	eBioscience	17-0451-83; RRID: AB_469393
TER-119 Monoclonal Antibody (TER-119), APC	eBioscience	17-5921-83; RRID: AB_469474
Anti-ERα Antibody (MC-20)	Santa Cruz	sc-542; RRID: AB_631470
Anti-Cytokeratin 8 Antibody, clone TROMA-1	Millipore Sigma	MABT329
Anti-SMO/Smoothened Antibody (E−5)	Santa Cruz	sc-166685; RRID: AB_2239686
Rabbit anti-PAX8 Antibody	Proteintech	10336-1-AP; RRID: AB_2236705
Mouse anti-Acetylated Tubulin Antibody	Millipore Sigma	T7451; RRID: AB_609894
Goat anti-Rabbit IgG (H + L) Highly Cross-Adsorbed Secondary Antibody, Alexa Fluor 594	Invitrogen	A-11037; RRID: AB_2534095
Goat anti-Rat IgG (H + L) Cross-Adsorbed Secondary Antibody, Alexa Fluor™ 594	Invitrogen	A-11007; RRID: AB_141374
Goat anti-Mouse IgG (H + L) Cross-Adsorbed Secondary Antibody, Alexa Fluor™ Plus 647	Invitrogen	A-21235; RRID: AB_2535804
Goat anti-Rabbit IgG (H + L) Highly Cross-Adsorbed Secondary Antibody, Alexa Fluor™ 647	Invitrogen	A-32733; RRID: AB_2633282
Goat anti-Mouse IgG (H + L) Highly Cross-Adsorbed Secondary Antibody, Alexa Fluor™ 594	Invitrogen	A-11005; RRID: AB_2534073
Chemicals, peptides, and recombinant proteins		
B27	Thermo Fisher Scientific	17504044
Human EGF	PeproTech	AF-100-15
TGF-β RI Kinase Inhibitor IV (SB431542)	Millipore Sigma	616464

(*Continued on next page*)

Continued

REAGENT or RESOURCE	SOURCE	IDENTIFIER
Y-27632 Rock Inhibitor	Sigma Aldrich	Y0503
Murine IGF1	PeproTech	250–19
Collagenase IV	Worthington Biochemical	Ls004188
Trypsin-EDTA	Signa-Aldrich	T4049
Matrigel	Corning	356231
Advanced DMEM/F-12 medium	Thermo Fisher Scientific	12634010
HEPES	Thermo Fisher Scientific	15630–80
GlutaMAX	Thermo Fisher Scientific	35050–061
TRIzol	Thermo Fisher Scientific	15596026
DNase I	Roche	10104159001
TrypLE Express	Thermo Fisher Scientific	12604013
DAPI	Sigma-Aldrich	D9542
Critical commercial assays		
iScript cDNA synthesis kit	Bio-RAD	170–8891
FastStart SYBR Green Master	Roche	04913850001
M.O.M.(TM) Basic Immunodetection Kit	Vector Laboratories	BMK-2202
Deposited data		
scRNA-seq data	GEO database	GSE194274
Experimental models: Organisms/strains		
FVB wild-type mouse	The Jackson Laboratory	Strain #001800; RRID: IMSR_JAX:001800
Rosa26-LSL-YFP (*R26Y*) reporter mouse	The Jackson Laboratory	Strain #006148; RRID: IMSR_JAX:006148
Pdgfra-Cre mouse	The Jackson Laboratory	Strain #013148; RRID: IMSR_JAX:013148
Oligonucleotides		
Ovgp1 forward: 5′ GCCCTTTCCCTCTTGTTCATA -3′	Xie et al.[40]	PMID: 30176443
Ovgp1 reverse: 5′ CCTGAGGCATTCACAGAAGAT -3′	Xie et al.[40]	PMID: 30176443
Pax8 forward: 5′ CCACCCTGACATCTTCCAATAC-3′	Xie et al.[40]	PMID: 30176443
Pax8 reverse: 5′ GTTTCCTGCTTTATGGCGAAG -3′	Xie et al.[40]	PMID: 30176443
Foxj1 forward: 5′ CTTCTTCCAGAACCTTCCTCTG -3′	Xie et al.[40]	PMID: 30176443
Foxj1 reverse: 5′ CCAGAACACTCACTTCCATTCT-3′	Xie et al.[40]	PMID: 30176443
Esr1 forward: 5′ CCTCCCGCCTTCTACAGGT-3′	Xie et al.[40]	PMID: 30176443
Esr1 reverse: 5′ CACACGGCACAGTAGCGAG -3′	Xie et al.[40]	PMID: 30176443
Lgr6 forward: 5′ GTCTTGTGGTGCTGCATCTA -3′	Xie et al.[40]	PMID: 30176443
Lgr6 reverse: 5′ GGAACTCCTGC AGCTCATTAT -3′	Xie et al.[40]	PMID: 30176443
Rspo1 forward: 5′ GGGATCAAGGGCAAGAGACAG-3′	This paper	N/A

(*Continued on next page*)

Continued

REAGENT or RESOURCE	SOURCE	IDENTIFIER
Rspo1 reverse: 5′ CTGGCGGATGTCGTTCCTC -3′	This paper	N/A
Wnt4 forward: 5′ AGACGTGCGAGAAACTCAAAG-3′	This paper	N/A
Wnt4 reverse: 5′ GGAACTGGTATTGGCACTCCT -3′	This paper	N/A
Wnt5a forward: 5′ CAACTGGCAGGACTTTCTCAA-3′	This paper	N/A
Wnt5a reverse: 5′ CATCTCCGATGCCGGAACT -3′	This paper	N/A
Software and algorithms		
Seurat single cell data analysis tool	Butler et al.[24]	https://satijalab.org/seurat/
Prism v9	Graphpad	https://www.graphpad.com/scientific-software/prism/
FlowJo 10.6.0	FlowJo LLC	https://www.flowjo.com/solutions/flowjo
CFX Maestro Software	BioRad	https://www.bio-rad.com/en-us/product/cfx-maestro-software-for-cfx-real-time-pcr-instruments?ID=OKZP7E15

RESOURCE AVAILABILITY

Lead contact

Further information and requests for the resources and reagents should be directed to and will be fulfilled by the Lead Contact, Zhe Li (zli4@rics.bwh.harvard.edu).

Materials availability

Further requests for resources and reagents should be directed to and will be fulfilled by the lead contact, Zhe Li (zli4@rics.bwh.harvard.edu). This study did not generate new unique reagents.

Data and code availability

- The scRNA-seq dataset generated during this study has been deposited to Gene Expression Omnibus (GEO) repository (https://www.ncbi.nlm.nih.gov/geo/) with the dataset identifier GSE194274.
- This paper does not report original code.
- Any additional information required to reanalyze the data reported in this paper is available from the lead contact upon request.

EXPERIMENTAL MODEL AND SUBJECT DETAILS

Mouse lines

All experimental procedures reported herein were reviewed and approved by our institutional animal care and use committee (IACUC), and performed in accordance with the relevant protocols (2016N000363 and 2020N000122). FVB stock mice [from The Jackson Laboratory (JAX) Strain #001800] were used as wild-type mice for scRNA-seq, flow cytometry, immunofluorescence, and real-time qRT-PCR. Mice entered the experiment between 8 and 12 weeks of age. No mice were excluded from the research. The *Rosa26-LSL-YFP* (*R26Y*) reporter mouse was acquired from JAX (#006148). The *Pdgfra-Cre* mouse was purchased from JAX (#013148). Since we study fallopian tube and ovary, only female mice were used as experimental mice.

METHOD DETAILS

Mouse FT and OS sample preparation for scRNA-seq

To perform single cell expression analysis of FT and ovary and to compare their transcriptomes, we isolated FT and ovarian tissues from WT adult FVB female mice. For FT, we cut each FT into two-halves and only subjected the distal half (i.e., the portion close to ovary) to single cell preparation. To isolate FT cells, FT tissues were dissected in dissection solution [PBS containing 2% fetal bovine serum (FBS) and 100 IU/mL of penicillin and 100 μg/mL Streptomycin]. After removing excessive connective and vascular tissues, the dissected FT tissues were minced into 1-2 mm pieces with an iris scissor or forceps, and then digested in 3.3 mg/mL collagenase IV (Worthington Biochemical #Ls004188) in DMEM/F12 medium for 1 h and 15 min at 37°C on a Nutating shaker. At the end of incubation, tissues were centrifuged at ~200–300 g for 5 min, and the pellets were then incubated with Trypsin-EDTA (Signa-Aldrich #T4049) and 1 mg/mL DNase I (Roche # 10104159001) sequentially, each for 5 min in a 37°C water bath. Cells were then passed through a 40 μm cell strainer to achieve a single cell suspension. FT cells were pelleted by centrifugation at ~200–300 g for 5 min at 4°C.

To isolate OS cells, ovaries were dissected and incubated with pre-warmed 0.25% Trypsin-EDTA (Signa-Aldrich #T4049) for 30 min at 37°C in a 5% CO_2 incubator. Care was taken not to agitate the ovaries. At the end of incubation, the supernatant containing stripped OS cells were transferred to a fresh tube, cells were triturated by gentle agitation by hand, and trypsin was inactivated by DMEM/F12 medium supplemented with 10% FBS. Stripped OS cells (enriched with OSE cells) were passed through a 100 μm cell strainer, followed by a 40 μm cell strainer to achieve a single cell suspension. OS cells were pelleted by centrifugation at ~200–300 g for 5 min at 4°C.

Generation of single-cell cDNA libraries and sequencing

We used the inDrop platform[23] to barcode single cells from FT and OS samples and to prepare expression libraries at the ICCB-L Single Cell Core, Harvard Medical School. After preparation of single cell suspensions, cells were encapsulated right away. Libraries were prepared with primers that includes 8-base (V3) long library index. Read 1 adaptor was on the 5′/cDNA (reads gene), and Read 2 adaptor was on the 3′ barcoded end (reads BC/UMI). V3 libraries were sequenced on Illumina NextSeq500 at the Dana-Farber Cancer Institute Molecular Biology Core Facilities. Raw sequencing data for each sample was converted to matrices of expression counts, after sample demultiplexing and barcode processing, by the Harvard Chan Bioinformatics Core.

scRNA-seq data analysis

The resulting UMI count matrix (genes x cells) were then provided as input to Seurat.[24] Quality control (QC) was performed to filter out the cells that have feature counts over 12,500 (doublets or multiplets), as well as feature counts less than 200 (dead/dying cells or an empty droplets). Cells that have more than 20% mitochondrial counts (damaged or dead cells) were also filtered out (Figure S1B). Single cells from both FT (i.e., FT#1 and FT#2 as FT) or OS (i.e., OS#1 and OS#2 as OS) samples were pooled. There were a total of 525 cells for FT samples and a total of 412 cells for OS samples; after QC, 372 cells for FT samples and 182 cells for OS samples were used in all subsequence analyses.

After removing unwanted cells from the dataset, LogNormalize method was utilized to normalize the data. Then the highly variable features were calculated using FindVariableFeature function, followed by a linear scaling transformation prior to downstream analysis, PCA. Clustering was performed using the FindClusters function with 0.5 resolution and integrated non-linear dimensional reduction (UMAP) visualization for all cells. Cluster-specific gene markers were identified using FindMarkers function with cutoffs avg-logFC>0.25. Doheatmap function was applied to generate expression heatmaps for given cells and features. Gene Set Enrichment Analysis (GSEA) for each cell cluster was conducted using the Molecular Signatures Database (MSigDB) (https://www.gsea-msigdb.org/gsea/msigdb), using the c2.cp or c2.cpg gene set collections, or using gene sets extracted from their corresponding publications.

Flow cytometry

Single cell suspensions from mouse FT tissues were analyzed by fluorescence-activated cell sorting (FACS) using BD FACSymphony (BD Biosciences) or FACS-sorted using BD FACSAria sorter (BD Biosciences). The cells were labeled with 1:100 antibodies and with DAPI for 15 min on ice. The antibodies used included

CD24 [Alexa Fluor® 700 Rat Anti-Mouse CD24 (BD Biosciences #564237), or CD24 Monoclonal Antibody (M1/69), Biotin (eBioscience #13-0242-82, followed by incubation with PerCP Streptavidin, BD Biosciences #554064)], CD66a [APC/Fire™ 750 anti-mouse CD66a (CEACAM1a) (Biolegend #134519), or FITC anti-mouse CD66a (CEACAM1a) Antibody (Biolegend #134517)], CD140a [CD140a (PDGFRA) Monoclonal Antibody (APA5), PE-Cyanine7 (eBioscience #25-1401-80)], CD61 [CD61 (Integrin beta 3) Monoclonal Antibody (2C9.G3), PE (eBioscience #12-0611-83)], and lineage markers including CD31 [CD31 (PECAM-1) Monoclonal Antibody (390), APC (eBioscience #17-0311-82)], CD45 [CD45 Monoclonal Antibody (30-F11), APC (eBioscience #17-0451-83)] and TER119 [TER-119 Monoclonal Antibody (TER-119), APC (eBioscience #17-5921-83)]. Data analyses were performed using FlowJo 10.6.0 (FlowJo LLC).

Organoid culture and co-culture

Single cell suspensions were embedded in 20 μL Matrigel (Corning #356231), resuspended, and allowed to solidify. The mixture was then overlaid with 250 μL pre-warmed BET or BETY organoid culture medium in one well of 48-well plate. BET medium refers to Advanced DMEM/F-12 medium (Thermo Fisher Scientific #12634010) with 10 mM HEPES (Gibco™ #15630-80), 1x GlutaMAX (Gibco^{TM} #35050-061), 100 IU/mL of penicillin and 100 μg/mL Streptomycin, 1x B27 (Thermo Fisher Scientific #17504044), 0.1 μg/mL human EGF (PeproTech #AF-100-15), 0.5 μM TGF-β RI Kinase Inhibitor IV (SB431542) (Millipore Sigma #616464). BETY medium refers to BET medium supplemented with 10 μM Y-27632 Rock Inhibitor (Sigma Aldrich #Y0503), which is only necessary when organoids are first prepared (from fresh tissues) or thawed. Organoids were grown at 37°C in a humidified atmosphere with 5% CO_2. The medium was changed once every 2–4 days, and the organoids were passaged at a ratio of 1:6 once every 10–14 days (or at a ratio of 1:2 once every 7 days). For passaging, the Matrigel containing the organoids was incubated in 1 mL TrypLE Express (Thermo Fisher Scientific #12604013) for 30 min, and then the single cell suspension was centrifuged for 5minat 1500rpmat 4°C. Appropriate number of cells from the resulting pellet was resuspended in cold Matrigel and reseeded in the 48-well tissue culture plate.

The organoid/stromal cell co-culture was established by seeding 4,000 FACS-sorted Lin^-CD24^+ FTE cells and 5,000 Lin^-CD24^- stromal cells from FT tissues of WT adult female mice. The freshly sorted Lin^-CD24^+ FTE cells either alone (4,000) or mixed together with Lin^-CD24^- stromal cells (5,000) and Matrigel were mixed using a pipette in a total volume of 15 μL. The mixture was added to the middle of the well to form a dome-like 3-dimentional structure and the plate was kept in the 37°C incubator for 10 min to solidify the Matrigel. After the mixture was solidified, 250 μL pre-warmed BET medium (initially in the presence of ROCK inhibitor) was added to each well. The resulting organoids were counted and measured 10 days after seeding.

To study the role of IGF1 in supporting the growth of FTE cells, FACS-sorted Lin^-CD24^+ FTE cells (4,000) were seeded in the BTY medium (i.e., removingEGF from the BETY medium) at the beginning, then changed to theBT medium (i.e., removingEGF from the BET medium) supplemented with 1 μg/mL Recombinant Murine IGF-I (PeproTech #250-19). Before changing the medium, 250 μL PBS was used to wash the surface of the Matrigel dome. The medium was changed once every 2–4 days.

Immunofluorescence

The dissected FT or ovary tissues were fixed in 10% formalin and embedded in paraffin. Immunofluorescent labeling was carried out by following standard procedures, by incubating tissue section with primary antibody for ERα (Santa Cruz #SC542, 1:50) diluted in PBS with 0.2% Tween and 0.5% Triton X-100, at 4°C overnight, or by incubating tissue section with primary antibodies for Smoothened (Santa Cruz #sc-166685, 1:100) and Cytokeratin 8 diluted in M.O.M reagent; the section was then washed with PBS-T (PBS with 0.1% Tween 20) or PBS (when M.O.M reagent was used), and incubated with the secondary antibody [Goat anti-Rabbit IgG (H + L) Highly Cross-Adsorbed Secondary Antibody, Alexa Fluor 594 (Invitrogen A11037)] (for ERα primary antibody), or incubated with the secondary antibodies [Goat anti-Rat IgG (H + L) Highly Cross-Adsorbed Secondary Antibody, Alexa Fluor 594 (Invitrogen A-11007) and Goat anti-Mouse IgG (H + L) Cross-Adsorbed Secondary Antibody, Alexa Fluor Plus 647 (Invitrogen A-21235)] (for Smoothened and Cytokeratin 8 primary antibodies), for 1 h at room temperature. After washing with PBS-T or PBS again, the sections were stained with DAPI.

For immunofluorescence staining on organoid section, the FT organoids with Matrigel were transferred to Histogel (Richard-Allan Scientific #HG-4000-012) and fixed in 10% formalin and embedded in paraffin.

Immunofluorescent labeling was carried out by following standard procedures, by incubating organoid sections with primary antibodies for PAX8 (Proteintech #10336-1-AP, 1:100) and Acetylated Tubulin (AcTUB) (Millipore Sigma #T7451, 1:1000) diluted in M.O.M diluent buffer (Vector Laboratories #BMK-2202), at room temperature for 30 min; the section was then washed with PBS, and incubated with the secondary antibodies [Goat anti-Rabbit IgG (H + L) Highly Cross-Adsorbed Secondary Antibody, Alexa Fluor 647 (Invitrogen A32733)] (for PAX8 primary antibody) and Goat anti-Mouse IgG (H + L) Highly Cross-Adsorbed Secondary Antibody, Alexa Fluor 594 (Invitrogen A-11005) (for AcTUB primary antibody)], for 30 min at room temperature. After washing with PBS again, the sections were stained with DAPI.

RNA quantification and real-time PCR

FT epithelial and stromal cell subpopulations were sorted based on FACS. The RNA was isolated with TRIzol (Thermo Fisher Scientific #15596026) according to the supplier's protocol. The amount and purify (based on the A260/280 ratio) were measured by NanoDrop Spectrophotometer (Thermo Fisher Scientific). Complete cDNA was synthesized from the isolated RNA by using iScript cDNA synthesis kit (Bio-RAD #170–8891). Real-time PCR was performed using the FastStart SYBR Green Master (Roche #04913850001). PCR reaction was performed in triplicate. The amplification plots obtained from the qRT-PCR were analyzed with CFX Maestro Software (BioRAD); expression levels were quantified by applying the comparative C (threshold cycle) method and calculating $\Delta\Delta$Ct. Relative expression levels of the target genes were normalized to the expression of glyceraldehyde-3-phosphate dehydrogenase (*Gapdh* gene) in each individual sample; in addition, the relative expression value of a target gene in each subpopulation of FT cells was calculated by normalizing to that in the $CD66a^{+}$ subpopulation (i.e., expression = 1).

QUANTIFICATION AND STATISTICAL ANALYSIS

All experiments were independently replicated at least three times. Statistical analysis was performed using Prism9, by Student's *t* test (for data with two treatment groups) or by ANOVA followed by a Tukey's analysis (for data with more than two treatment groups). Data were reported as Mean $\pm$ SEM unless otherwise indicated. Qualitative images presented are representative of the outcomes obtained in the replicate experiments.